Max-Planck-Institut
für Meteorologie

MAX-PLANCK-GESELLSCHAFT

International Max Planck Research School
on Earth System Modelling

Interactions between climate and vegetation at high northern latitudes during the mid-Holocene

Juliane Otto

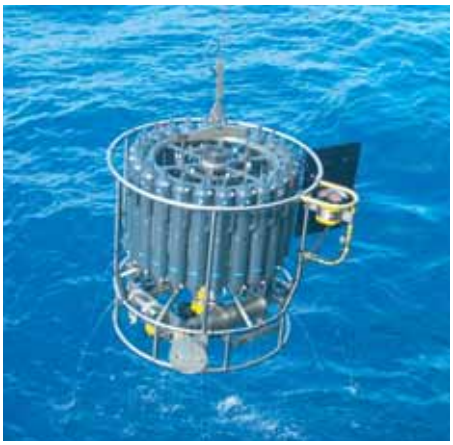

Berichte zur Erdsystemforschung 80
2010

Reports on Earth System Science

Hinweis

Die Berichte zur Erdsystemforschung werden vom Max-Planck-Institut für Meteorologie in Hamburg in unregelmäßiger Abfolge herausgegeben.

Sie enthalten wissenschaftliche und technische Beiträge, inklusive Dissertationen.

Die Beiträge geben nicht notwendigerweise die Auffassung des Instituts wieder.

Die "Berichte zur Erdsystemforschung" führen die vorherigen Reihen "Reports" und "Examensarbeiten" weiter.

Notice

The Reports on Earth System Science are published by the Max Planck Institute for Meteorology in Hamburg. They appear in irregular intervals.

They contain scientific and technical contributions, including Ph. D. theses.

The Reports do not necessarily reflect the opinion of the Institute.

The "Reports on Earth System Science" continue the former "Reports" and "Examensarbeiten" of the Max Planck Institute.

Anschrift / Address

Max-Planck-Institut für Meteorologie
Bundesstrasse 53
20146 Hamburg
Deutschland

Tel.: +49-(0)40-4 11 73-0
Fax: +49-(0)40-4 11 73-298
Web: www.mpimet.mpg.de

Layout:

Bettina Diallo, PR & Grafik

Titelfotos:
vorne:
Christian Klepp - Jochem Marotzke - Christian Klepp
hinten:
Clotilde Dubois - Christian Klepp - Katsumasa Tanaka

Berichte zur Erdsystemforschung 80/2010

Interactions between climate and vegetation at high northern latitudes during the mid-Holocene

Juliane Otto

aus Greifswald

Hamburg 2010

Reports on Earth System Science 80/2010

ISSN 1614-1199

Juliane Otto
Max-Planck-Institut für Meteorologie
Bundesstrasse 53
20146 Hamburg
Germany

Als Dissertation angenommen
vom Department Geowissenschaften der Universität Hamburg

auf Grund der Gutachten von
Prof. Dr. Martin Claussen
und
Dr. Thomas Raddatz

Hamburg, den 25. Juni 2010
Prof. Dr. Jürgen Oßenbrügge
Leiter des Departments für Geowissenschaften

ISSN 1614-1199

Interactions between climate and vegetation at high northern latitudes during the mid-Holocene

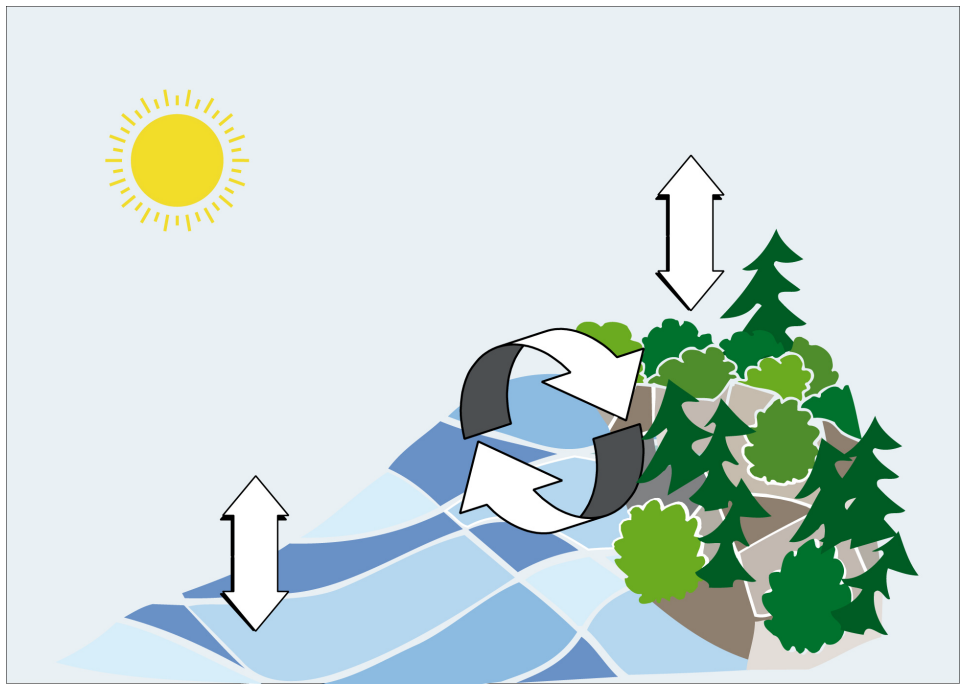

Juliane Otto

Hamburg 2010

Abstract

The mid-Holocene climate, about 6000 years before present, is investigated with the comprehensive general circulation model ECHAM5/JSBACH-MPIOM at high northern latitudes. Applying a factor-separation technique, we isolate the contributions of the atmosphere, the atmosphere-vegetation feedback, the atmosphere-ocean feedback and their synergy to the mid-Holocene climate change signal.

The mid-Holocene climate signal shows a modification of the seasonal cycle at the high northern latitudes compared to pre-industrial climate. This is characterised by increased temperatures in summer, autumn and winter, and a cooler climate in spring. The summer warming is primarily caused by the direct response of the atmosphere to the change in insolation. The autumn temperature rise, however, results not only from the direct atmospheric signal but is also amplified by the atmosphere-ocean feedback. The winter warming is primarily induced by the atmosphere-ocean feedback, counteracting the cooling caused by the the direct atmospheric signal. In spring, the temperature decrease is a combined effect of the direct atmospheric signal and the atmosphere-ocean feedback. The atmosphere-vegetation feedback compensates this cooling only marginally. The synergy between the atmosphere-ocean and atmosphere-vegetation feedback results in slight warming for all seasons. In summary, the direct mid-Holocene climate response to the change in insolation is mainly modified by the atmosphere-ocean feedback. In contrast, the atmosphere-vegetation feedback influences the mid-Holocene climate signal only marginally.

We test the statistical robustness of the results. The atmosphere response and the atmosphere-vegetation feedback are statistically robust. By contrast, the factors derived from simulations with an interactive ocean are sensitive to long-term anomalies in sea-ice cover. Nevertheless, the statistical testing confirms that the most important modification of the direct climate response to the orbital forcing can be related to the atmosphere-ocean feedback.

A detailed analysis of the atmosphere-vegetation feedback shows that the expansion of forest during the mid-Holocene causes two opposing effects in spring. On the one hand, the increase in forest results in a reduction in surface albedo and, thus, enhances the absorption of solar radiation which leads to a near-surface air-temperature rise. On the other hand, the expansion of forest favours the increase in transpiration and, thus, an increase in cloud fraction, which, in turn, dampens the warming signal. Furthermore, it is investigated to what extent the strength of the atmosphere-vegetation feedback depends on the parametrisation of the albedo of snow. A parametrisation with a strong reduction in the albedo of snow by deciduous trees increases the temperature signal regionally. Simulations with the albedo of snow depending on the age of snow show a regional increase in temperature as well. However, the large-scale temperature signal of the atmosphere-vegetation feedback simulated with ECHAM5/JSBACH remains weak compared to previous studies.

Zusammenfassung

Das Klima des mittleren Holozäns, vor ungefähr 6000 Jahren, wird mit dem komplexen Zirkulationsmodell ECHAM5/JSBACH-MPIOM für die hohen nördlichen Breiten untersucht. Eine Faktorenseparationstechnik wird angewandt, um die Beiträge der Atmosphäre, der Rück-kopplung zwischen Atmosphäre und Vegetation, sowie zwischen Atmosphäre und Ozean und deren Synergie zum Klimasignal des mittleren Holozäns zu bestimmen.

Das Klimasignal des mittleren Holozäns zeigt eine Änderung des saisonalen Zyklus in den hohen nördlichen Breiten im Vergleich zum präindustriellen Klima. Dies äußert sich in erhöhten Temperaturen im Sommer, Herbst und Winter, und in einer Abkühlung im Frühling. Die sommerliche Erwärmung ist hauptsächlich ein Ergebnis der direkten Reaktion der Atmosphäre auf die Änderung der Einstrahlung. Der Temperaturanstieg im Herbst wird hingegen nicht nur durch das direkte Signal der Atmosphäre verursacht, sondern zusätzlich durch die Rückkopplung zwischen Atmosphäre und Ozean verstärkt. Die Erwärmung im Winter wird hauptsächlich durch die Rückkopplung zwischen Atmosphäre und Ozean hervorgerufen, deren Beitrag der Abkühlung durch das direkte Atmosphärensignal entgegenwirkt. Im Frühling wird die Temperaturabnahme durch das direkte Atmosphärensignal und der Rückkopplung zwischen Atmosphäre und Ozean hervorgerufen. Die Rückkopplung zwischen Atmosphäre und Vegetation kompensiert diese Abkühlung nur geringfügig. Die Synergie zwischen den Rückkopplungen führt zu einer leichten Erwärmung in allen Jahreszeiten. Zusammengefasst lässt sich festhalten, dass die direkte Reaktion des Klimas des mittleren Holozäns auf die Änderung der Einstrahlung hauptsächlich durch die Rückkopplung zwischen Atmosphäre und Ozean modifiziert wird. Die Rückkopplung zwischen Atmosphäre und Vegetation hingegen beeinflusst das Klimasignal des mittleren Holozäns nur geringfügig.

Die statistische Robustheit der Ergebnisse wird getestet. Die atmosphärische Reaktion und die Rückkopplung zwischen Atmosphäre und Vegetation sind statistisch robust. Im Gegensatz dazu reagieren die Faktoren, die aus Simulationen mit einem interaktiven Ozean berechnet worden sind, empfindlich gegenüber Langzeitanomalien des Meereises. Dennoch bestätigt der statistische Test, dass die direkte Klimareaktion auf das orbitale Signal hauptsächlich durch die Rückkopplung zwischen Atmosphäre und Ozean modifiziert wird.

Eine detailierte Analyse der Rückkopplung zwischen Atmosphäre und Vegetation zeigt, dass die Ausbreitung des Waldes im mittleren Holozän zwei Effekte hervorruft, die gegensätzlich auf die Temperatur im Frühling wirken. Auf der einen Seite bewirkt der Zuwachs an Wald eine Reduktion der Bodenalbedo, wodurch die Absorption der solaren Strahlung zunimmt, was einen Temperaturanstieg zur Folge hat. Auf der anderen Seite führt der Waldzuwachs zu einer Zunahme der Transpiration und damit zu einer Zunahme an Bewölkung, was das Erwärmungssignal abschwächt. Darüber hinaus wird untersucht bis zu welchem Grad die Stärke der Rückkopplung zwischen Atmosphäre und Vegetation von der Parametrisierung der Albedo des Schnees abhängt. Eine Parametrisierung mit einer starken Reduzierung der Albedo des Schnees durch laubabwerfende Bäume verstärkt regional das Temperatursignal. Simulationen mit einer Albedo des Schnees, die von dem Alter des Schnees abhängt, zeigen ebenso eine regionale Erhöhung der Temperatur. Das mit ECHAM5/JSBACH simulierte großskalige Temperatursignal der Rückkopplung zwischen Atmosphäre und Vegetation bleibt jedoch schwach im Vergleich zu vorhergehenden Studien.

Contents

Chapter 1

Introduction

Studies based on model simulations of past climates (e.g. Foley et al. (1994); deNoblet et al. (1996); Claussen et al. (1999); Brovkin et al. (2003); Gallimore et al. (2005); Renssen et al. (2009)) have contributed considerably to our understanding of the role feedbacks play in the climate system. The benefit of such analyses is threefold: (1) they examine the role of climate feedbacks under various external forcings, (2) they evaluate the capability of climate models to reproduce climate states that are different from those of today, (3) they help us to get a globally and physically consistent picture of past climate change. Considering these benefits, the aim of this thesis is to enhance the understanding of feedbacks between the components of the climate system at high northern latitudes.

As an external forcing we use the differences in insolation between today and the mid-Holocene, which is the climate period about 6000 years before present. At this time, the insolation was increased during summer by 5% and decreased in winter by 5% over the Northern Hemisphere, due to changes in the Earth's orbit (Berger 1978). Palaeo-reconstructions indicate that the summer and autumn were warmer by up to 4 °C throughout much of the high-latitude Northern Hemisphere. As a consequence, the boreal forest was positioned north of its present location in many regions (Cheddadi et al. 1996; Kerwin et al. 1999; Bigelow et al. 2003). In winter, the case was different compared to summer and autumn. Despite the decrease in winter insolation compared to today, Cheddadi et al. (1996) report higher than present winter temperatures in North-East Europe by up to 3 °C. Furthermore, Davis et al. (2003) suggest not only warmer winter but higher annual mean temperatures for northern Europe by up to 1.4 °C compared to present-day climate. These warming signals cannot be directly explained by changes in orbital configurations. Therefore the climate response to the changes in insolation must have been altered by other mechanisms.

In order to determine these mechanisms, simulations with interactive atmosphere-ocean-vegetation models can be utilised. A factor-separation technique (Stein and Alpert 1993; Berger in press) allows us to study the pure contributions of the atmosphere, the vegetation and the ocean and the synergy between them to the climate change signal. In this study, we apply this technique by using the atmosphere-vegetation-ocean general circulation model (GCM) to investigate the contribution of the vegetation and the ocean to the mid-Holocene climate change. We refer to these contributions as

the atmosphere-vegetation and atmosphere-ocean feedback, respectively. In our definition, the term "feedback" includes all interactions between the atmosphere and the land-surface and between the atmosphere and the ocean including sea-ice, respectively. Single feedback loops, e.g. the sea ice-albedo feedback, are defined in the 'classical way' (Bates 2007). After iteration, they change the climate in the same (positive feedback) or opposite direction (negative feedback) as the trigger that initiated them. We refer to such single feedback loops explicitly.
So far, the complete factor-separation technique has been applied only by mid-Holocene studies with Earth system models of intermediate complexity (EMICs). Ganopolski et al. (1998), using an EMIC show that the synergy between the atmosphere-ocean and the atmosphere-vegetation feedback is stronger than their pure contributions. There are only few mid-Holocene simulations with General Circulation Models (GCMs) including dynamic representations of the global atmosphere, ocean and vegetation (Braconnot et al. 2007a). Using a GCM asynchronously coupled with a vegetation model and applying the factor-separation technique in parts, Wohlfahrt et al. (2004) suggest a stronger atmosphere-vegetation feedback but a weaker synergy than analysed by Ganopolski et al. (1998). Results from the Paleoclimate Modelling Intercomparison Project (PMIP2) with EMICs and GCMs (Braconnot et al. 2007a,b) corroborate that the atmosphere-ocean feedback plays a major role in altering the climate response to insolation change. However, it is not possible to deduce the relative role of neither the atmosphere-ocean feedback nor of the atmosphere-vegetation feedback from PMIP2-simulations. As none of the previous studies with GCMs followed the factor-separation technique with consistency, the main research question of this study is:

(1) Using a comprehensive GCM and applying the factor-separation technique, how do we relate the mid-Holocene climate signal to the components of the climate system?

Joussaume and Braconnot (1997) stated that when modelling past climates, we need to address the question of defining a calendar for past periods. The precessional cycle and changes in the eccentricity of the Earth's orbit induce changes in the length of the seasons. If the seasons are not defined consistently with the insolation forcing, biases may be introduced artificially when comparing model results of two different climatic periods. As we compare mid-Holocene with pre-industrial simulations, we define the seasons by astronomical dates: vernal and autumn equinox, summer and winter solstice (Timm et al. 2008). To our knowledge, none of the high-latitude mid-Holocene studies has considered this issue before (Braconnot et al. 2007a,b). Therefore, we ask the following question:

(2) Does the definition of the seasons effect the assignment of the mid-Holocene climate signal to the components of the climate system?

Although most of the previous mid-Holocene studies have not followed a complete factor separation technique, they have suggested that the response of the ocean and the vegetation to mid-Holocene insolation feeds back on the climate. There is less consensus, however, on the relative magnitude of the two feedbacks and the strength of the synergy between them. These divergent results may be ascribed to differences in the structure and parameterisation of the models as well as to the setup of the simulations. On the other hand, models exhibit internal variability due to nonlinearities in the model physics and dynamics (Murphy et al. 2004). Therefore, the question arises how much of the differences among the results of model studies can be attributed to sampling variability. Commonly, experiments are spun up until the climate trends are small, then the last 100 to 200 years are analysed (Braconnot et al. 2007a). Analysing a period of this length may not account for long-term climate variability, thus introducing uncertainty in the diagnosed feedbacks. Thus, we attempt to answer the question:

(3) Does statistical uncertainty introduced by climate variability lead to divergent model results?

Another explanation for the divergent model results may be the difference in structure and parameterisation of the land surface in the utilised climate models. Bony et al. (2006) stated in a review article that the main difference between climate models arises from the way the albedo of snow is parametrised in the models. A study comparing 18 GCMs revealed that the models differ in the strength of the snow-albedo feedback because of the various snow-albedo parametrisations (Qu and Hall 2007). Levis et al. (2007) showed that in their simulations two equally justifiable snow-cover parametrisations can lead to a 0.2 °C difference in climate sensitivity. Thus, the discrepancy between modelling results on mid-Holocene feedbacks may arise from systematic errors due to different land-surface model parameterisations. To test this hypothesis, we first investigate the atmosphere-vegetation feedback in detail to understand the processes which are involved in this feedback. Secondly, we investigate the sensitivity of the atmosphere-vegetation feedback with respect to the parameterisation of the albedo of snow-covered land. Thus, we perform several sets of simulations with different snow-albedo parametrisations to examine how they influence the mid-Holocene climate signal. By doing this, we want to answer to question:

(4) To what extent does the strength of the atmosphere-vegetation feedback depend on the snow-albedo parametrisation?

In Chapter 2, we introduce the experimental design following the factor-separation technique. With the results and the discussion of Chapter 2, we address the above-defined research questions (1) and (2). In Chapter 3, we investigate the statistical

uncertainty introduced by climate variability, addressing the research questions (3). Chapter 2 and Chapter 3 have been published in *Geophysical Research Letters* [1] [2]. In Chapter 4, we concentrate on the role of the atmosphere-vegetation feedback and investigate how different parametrisations of the albedo of snow influence the strength of the atmosphere-vegetation feedback, addressing the research questions (4) and (5). We present our conclusions and an outlook in Chapter 5.

[1] Otto, J., Raddatz, T., Claussen, M., Brovkin, V., and Gayler, V.: Separation of atmosphere-ocean-vegetation feedbacks and synergies for mid-Holocene climate, Geophysical Research Letters, 36, L09 701, 2009b.

[2] Otto, J., Raddatz, T., and Claussen, M.: Climate variability-induced uncertainty in mid-Holocene atmosphere-ocean-vegetation feedbacks, Geophysical Research Letters, 36, L23 710, 2009a.

Chapter 2

Separation of atmosphere-ocean-vegetation feedbacks and synergies for mid-Holocene climate

2.1 Introduction

The mid-Holocene, around 6000 years before present (6 ka), is a common reference period to examine the climate response to changes in incoming solar radiation caused by variations in the Earth's orbit (Braconnot et al. 2007a,b). The mid-Holocene orbital changes led to an increase in insolation during summer and beginning of autumn and a decrease in winter in the Northern Hemisphere compared to present day (Berger 1978). As a consequence, during the mid-Holocene the Northern Hemisphere summers were warmer than at present day as shown e.g. by Davis et al. (2003) with pollen-based climate reconstructions. These reconstructions also indicate higher mid-Holocene annual mean temperatures for the high northern latitudes. The annual mean insolation, however, changed only marginally. Thus, the seasonal insolation changes amplified by feedbacks may have caused this annual mean signal. To test this assumption, we present results of a factor-separation technique applied to a state-of-the-art climate model.
The climate of the high northern latitudes are controlled by several feedbacks involving e.g. changes in the hydrological cycle, heat-flux or albedo. Two positive albedo-related feedbacks presumably have the strongest impact on climate in response to orbitally-induced changes: the taiga-tundra feedback and the sea ice-albedo feedback. The taiga-tundra feedback, includes that forest effectively masks out high albedo in comparison with tundra. A replacement of tundra by forest decreases the surface albedo during the snowy season which leads to a warming and favours further growth of boreal forest. The sea ice-albedo feedback functions in a similar way: a reduction in sea-ice cover in response to increasing temperatures leads to less sea ice and thus to lower surface albedo and further warming (Harvey 1988). The taiga-tundra and sea ice-albedo feedback may amplify each other and cause a more pronounced warming (Claussen et al. 2006).

However, such climate sensitivity to orbital forcing is not well understood. Previous studies on the impact of feedbacks altering the response of climate to mid-Holocene orbital forcing have shown differing results. A factor-separation technique (Stein and Alpert 1993) can be used to estimate the role of feedbacks. So far, it has been applied only by studies with Earth system models of intermediate complexity (EMICs). With the CLIMBER-2 model Ganopolski et al. (1998) showed that the synergy between the atmosphere-ocean and atmosphere-vegetation feedback is stronger than their pure contributions and that this synergy leads to an annual mid-Holocene warming.
There are only few mid-Holocene simulations with General Circulation Models (GCMs) including dynamic representations of the global atmosphere, ocean and vegetation (Braconnot et al. 2007a). Using a GCM asynchronously coupled with a vegetation model and partly applying the factor-separation technique, Wohlfahrt et al. (2004) depict warmer mid-Holocene than pre-industrial climate throughout the year. They suggest that atmosphere-vegetation feedback and the synergy between atmosphere-vegetation and atmosphere-ocean feedback produce warming in all seasons. Their results suggest a stronger atmosphere-vegetation feedback but a weaker synergy than analysed by Ganopolski et al. (1998). Results from the Palaeoclimate Modelling Intercomparison Project (PMIP2) with EMICs and GCMs (Braconnot et al. 2007a,b) corroborate that the atmosphere-ocean feedback plays a major role in altering the response to insolation change. It is not possible to conclude on the relative role of the atmosphere-vegetation feedback from PMIP2-simulations. Notwithstanding, Braconnot et al. (2007b) assume that the magnitude of the atmosphere-vegetation feedback is smaller than previously discussed.
None of the previous studies with GCMs followed consistently the factor-separation technique. We apply this technique to a complete set of simulations with a coupled atmosphere-ocean-vegetation GCM to separate the atmosphere-vegetation feedback and the atmosphere-ocean feedback from their synergy term.

2.2 Setup of Model Experiments

We performed our numerical experiments with the atmosphere-ocean GCM ECHAM5-MPIOM including the land surface scheme JSBACH with a dynamic vegetation module. The spectral atmosphere model ECHAM5 was run in T31 resolution (approx. 3.75°) with 19 vertical levels, the ocean model MPIOM in a resolution of roughly 3° and 40 vertical levels (Jungclaus et al. 2006) without any flux adjustment. The land surface scheme JSBACH is presented in Raddatz et al. (2007). It was extended with a dynamic vegetation module (Brovkin et al. 2009). The experiment set-up was designed to follow the factor-separation technique by Stein and Alpert (1993). By applying this technique we are able to determine the contributions of interactions between different components of the climate subsystem and their synergistic effects to a climate change signal (Berger 2001). In this study, we focus on two interactions: the atmosphere-ocean and the atmosphere-vegetation feedback. Firstly, the four pre-industrial climate simulations

experiment name	prescribed from which experiment	length
pre-industrial		
0kAOV	–	620 years
0kAO	vegetation, *0kAOV*	620 years
0kAV	SST, sea ice, *0kAOV*	360 years
0kA	SST, sea ice, *0kAOV* vegetation, *0kAV*	140 years
mid-Holocene		
6kAOV	–	620 years
6kAO	vegetation, *0kAOV*	620 years
6kAV	SST, sea ice, *0kAOV*	360 years
6kA	SST, sea ice, *0kAOV* vegetation, *0kAV*	140 years

Table 2.1: Setup of experiments

were performed: an equilibrium atmosphere-ocean-vegetation simulation (*0*kAOV), an equilibrium atmosphere-ocean simulation (*0*kAO) with vegetation prescribed (as fraction of each vegetation type and of desert) from *0*kAOV, a simulation with interactive atmosphere and vegetation dynamics (*0*kAV) with sea-surface temperature (SST) and sea-ice cover prescribed as monthly mean values of the *0*kAOV-simulation, and an atmosphere-only simulation (*0*kA) preformed as *0*kAV but with vegetation prescribed from this run *0*kAV. Secondly, the mid-Holocene simulations were performed: *6*kAOV, *6*kAO, *6*kAV, *6*kA. These simulations were carried out in an analogous manner to the pre-industrial simulations but with respective mid-Holocene orbital parameters, and vegetation cover, the seasonal cycle of SST and sea-ice cover, if prescribed, were taken from the pre-industrial simulations (Table 2.1). Because of non-linearity in our model, we do not refer to only one controll run in contrast to studies with EMICs.

All simulations were performed with atmospheric CO_2 concentrations set to 280 ppm. The simulations with dynamic ocean were run for 620 years, with prescribed ocean accordingly shorter (Table 2.1). For the analysis, the last 120 years of all experiments were considered.

With these simulations, we quantify the contribution of interactions between the atmosphere-ocean and atmosphere-vegetation dynamics to the mid-Holocene climate. The deviation between the fully coupled runs in terms of temperature (ΔAOV) contains all feedbacks and synergistic effects. It is obtained by

$$\Delta AOV = 6kAOV - 0kAOV. \tag{2.1}$$

The response of the atmosphere (ΔA) is determined as follows

$$\Delta A = (6kA - 0kA). \tag{2.2}$$

By comparing the results in AV and AO with those from A, it is possible to assess the contribution of the atmosphere-vegetation (ΔV) and the atmosphere-ocean feedback (ΔO):

$$\Delta V = (6kAV - 0kAV) - (6kA - 0kA) \tag{2.3}$$

$$\Delta O = (6kAO - 0kAO) - (6kA - 0kA). \tag{2.4}$$

The synergistic effects (ΔS) between atmosphere-vegetation and atmosphere-ocean feedback can be quantified as the difference between ΔAOV and the sum of the three components atmosphere ΔA, ocean ΔO and vegetation ΔV:

$$\Delta S = \Delta AOV - \Delta A - \Delta O - \Delta V. \tag{2.5}$$

In order to keep the definition of seasons consistent with insolation forcing in pre-industrial and mid-Holocene climate, an astronomically based calendar is necessary (Joussaume and Braconnot 1997). Accordingly, we considered the seasons defined by astronomical dates: vernal equinox, summer solstice, autumn equinox, winter solstice. Since an astronomical calendar is not implemented in our model, we calculated the seasons from the daily output according to the model's astronomical parameters for pre-industrial and for mid-Holocene climate respectively (Timm et al. 2008). In previous mid-Holocene studies, seasons have been determined by monthly means which were computed with the present-day calendar. To compare our results with previous studies we shifted the seasons backwards by three weeks relative to the astronomical season. Seasonal averages are then computed from the daily output of the model for the pre-industrial and the mid-Holocene period, respectively.

2.3 Results

Despite the small annual mean insolation anomalies in the northern latitudes (1.40 W/m^2 $\geq$ 40°N), the annual mean mid-Holocene temperature is distinctly increased in comparison to pre-industrial climate, which is in agreement with e.g. climate reconstructions for Northern Europe (Davis et al. 2003). The fully coupled model including all feedbacks and synergies shows a general annual mid-Holocene warming with values of up to 4 °C around Greenland (Figure 2.1, ΔAOV). The temperature pattern in Figure 2.1 (ΔA) shows the response of the atmosphere only to the orbital signal without atmosphere-ocean and atmosphere-vegetation feedbacks. It results in a slight warming but only for the continents with maximum values in Greenland of up to 1 °C (Figure 2.1, ΔA). This reveals that the larger obliquity results in a weak annual temperature increase. Vegetation dynamics also lead to continental warming (Figure 2.1,

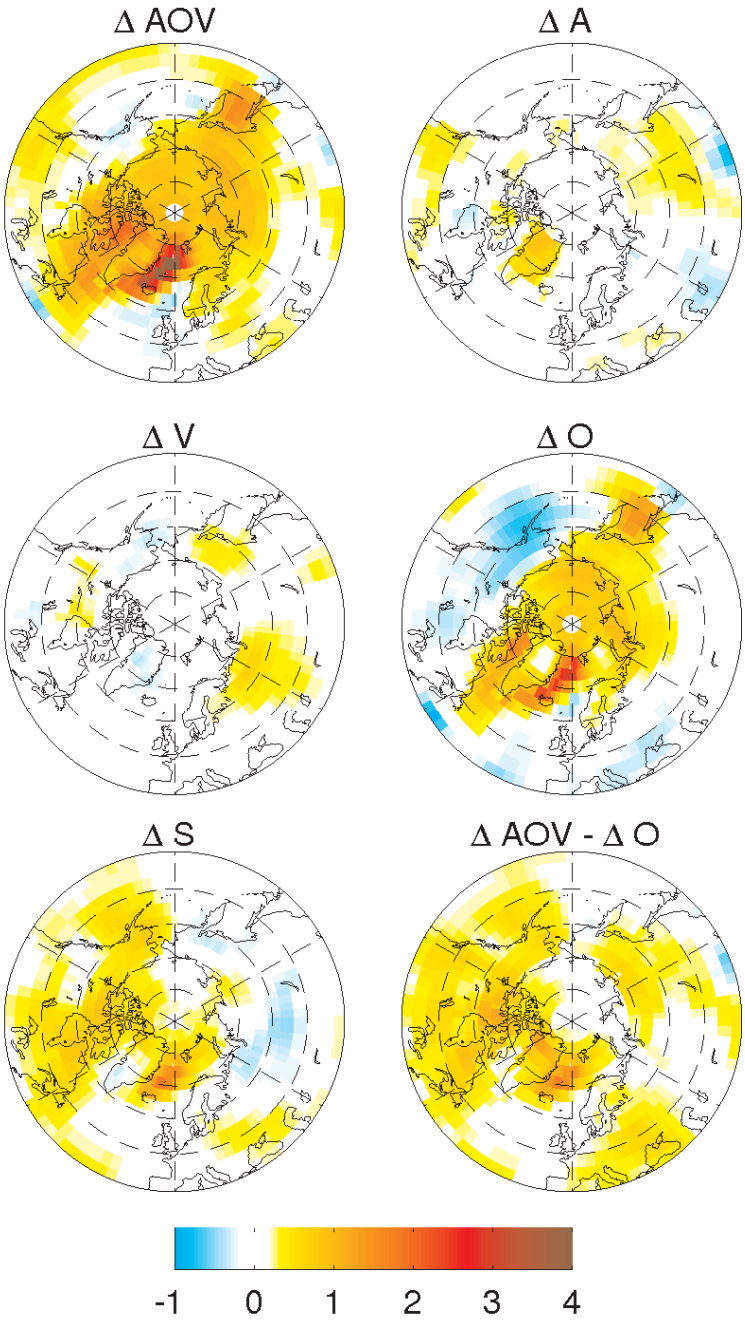

Figure 2.1: Annual mean 2m-temperature anomalies [°C] between 6 ka and 0 ka according to ΔAOV, ΔA, ΔV, ΔO and ΔS.

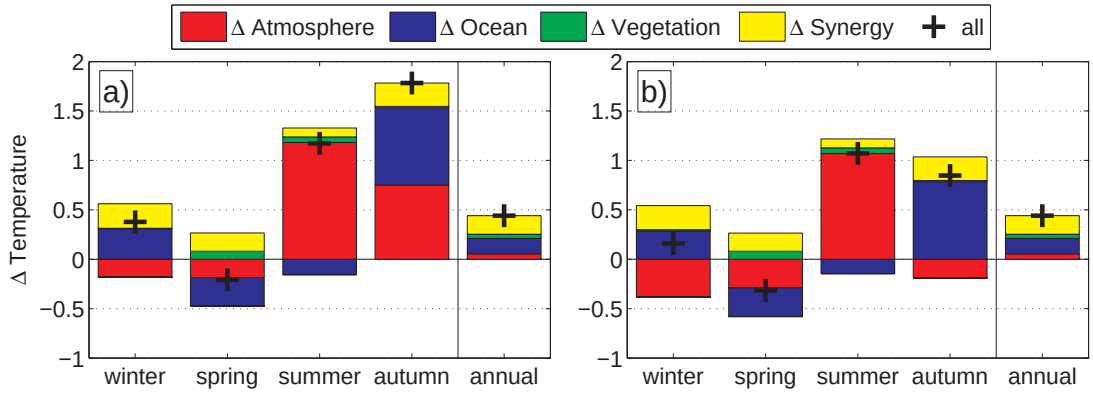

Figure 2.2: Seasonal temperature anomalies [°C] between 6 ka and 0 ka of the coupled simulations ΔAOV (+) and the contributions of the factors ΔA (red), ΔV (green), ΔO (blue) and ΔS (yellow) to the signal in seasonal temperature, NH $\geq 40°$. (a) Seasons are defined on an astronomical basis. Note: Because of the astronomically based calendar, the length of the seasons differ between 0k and 6k. Thus the annual mean is not the linear average of the seasonal means. (b) Seasons are defined by present-day calendar but the date of the vernal equinox is fixed on the 21 March (as done by PMIP2-simulations).

ΔV), however it is less pronounced. Compared to ΔA, vegetation dynamics lead to a warming of west Siberia with maximum values of up to 0.6 °C and a cooling of Greenland. The atmosphere-ocean feedback ΔO (Figure 2.1, ΔO) however shows a slightly cooler but similar temperature pattern as the fully coupled model (Figure 2.1, ΔAOV and $\Delta AOV - \Delta O$). The synergy ΔS (Figure 2.1, ΔS) between atmosphere-vegetation and atmosphere-ocean feedback adds additional warming with maximum values of up to 2 °C around Greenland. The separation technique reveals that mean annual warming is not only caused by larger obliquity and changes in precession but rather by the atmosphere-ocean feedback and the synergy between the atmosphere-ocean and the atmosphere-vegetation feedback.

To analyse the climatic response to change in orbital forcing more closely, we focus on the seasonal cycle of temperature. Figure 2.2 depicts the seasonal cycle of the 2m-temperature of ΔAOV together with contributions of the single feedbacks ΔA, ΔO, ΔV and their synergy ΔS. Our results show an amplification of the seasonal cycle of the Northern Hemisphere 2m-temperature ($\geq 40°$N), as expected from the orbital-induced change in insolation. This is characterised by increased 2m-temperature in summer, autumn and winter, and its decrease in spring (Figure 2.2a). The direct response of the atmosphere (ΔA) to the change in insolation produces a summer warming of 1.18 °C which slightly decreases in autumn to 0.75 °C. However, winter and spring seasons show a cooling of -0.18 °C and -0.19 °C respectively. The atmosphere-vegetation feedback ΔV is rather marginal. In spring and summer it leads to a slight warming of 0.08 °C and 0.06 °C respectively counteracting to the insolation changes. Atmosphere-ocean feedbacks amplify the response to the orbital forcing in spring and autumn and counteract the direct response slightly in summer and more strongly in winter. The

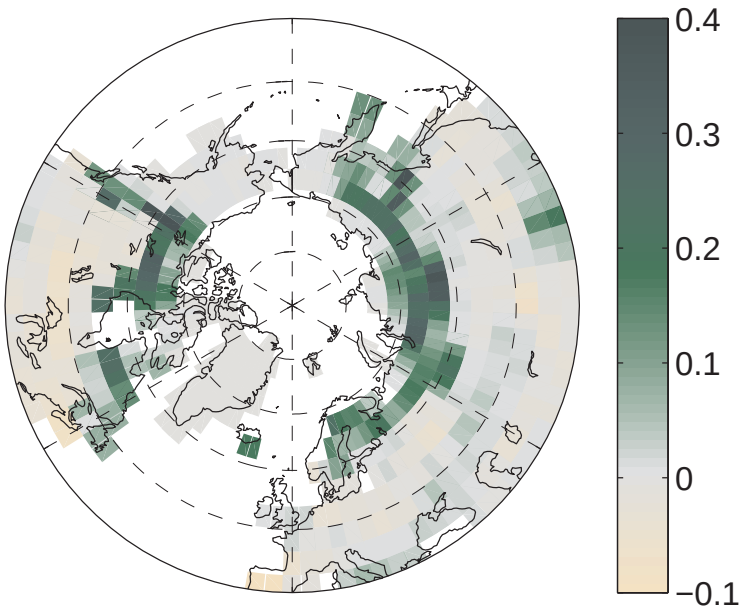

Figure 2.3: Annual change in forest cover between 6 ka and 0 ka (ΔAOV).

ocean's influence on the warming of the northern latitudes is strongest in autumn (0.78 °C), reflecting the orbitally induced increase in summer and autumn insolation. The atmosphere-ocean contribution continues with 0.30 °C in winter, resulting likely from the thermal inertia of the ocean that introduces a lag between the season cycle of insolation and oceanic response by approximately one season. The synergy between the atmosphere-ocean and atmosphere-vegetation feedback results in slight warming for all seasons. The maximum contribution of the synergy occurs in autumn and winter with a warming of 0.24 °C and 0.25 °C respectively; the weakest in summer with 0.09 °C. In summary, the seasonal temperature pattern shows that the atmosphere-ocean feedback modulates the mid-Holocene insolation forcing whereas the amplifying prevails over damping. The contribution of the atmosphere-vegetation feedback remains marginal throughout the year. The synergy between the atmosphere-ocean and atmosphere-vegetation feedback however leads to a slight warming in all seasons.

2.4 Discussion

Our results reveal that atmosphere-ocean and atmosphere-vegetation feedback and their synergy modify the orbitally-induced pattern of seasonal temperature considerably. The modification leads to an annual mean warming in the high latitudes of 0.44 °C (Figure 2.2a). Results of the model CLIMBER-2 for the Northern Hemisphere (Ganopolski et al. 1998) and the IPSL model (Wohlfahrt et al. 2004) north of 40°N show a considerably stronger annual warming of up to 1 °C. Besides, the seasonal temperature signals

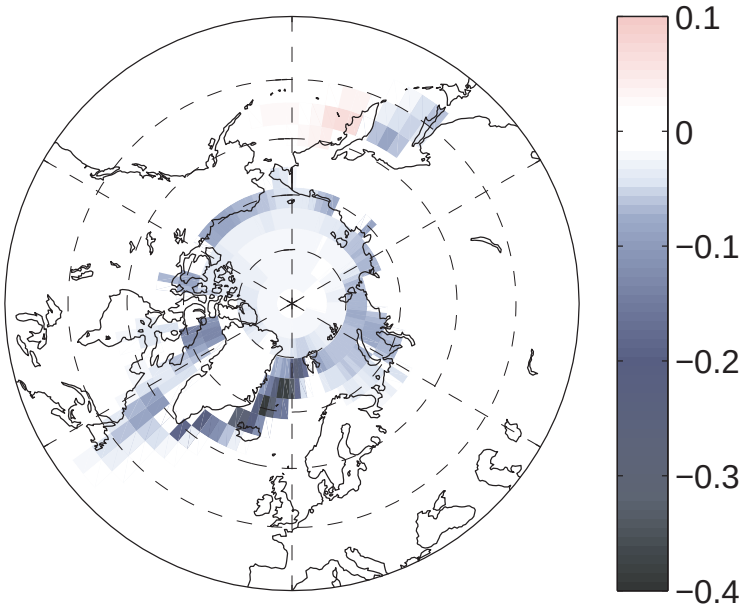

Figure 2.4: Annual change in sea-ice cover change between 6 ka and 0 ka (ΔAOV). The change in sea-ice cover ΔAO exhibits similar patterns (not shown).

differ in phase and magnitude. Our model shows that the maximum warming occurs in autumn, contrary to previous studies (Gallimore et al. 2005; Wohlfahrt et al. 2004) which suggest a maximum warming in summer. Figure 2.2a shows that the atmosphere autumn response is doubled by the amplification of the atmosphere-ocean interactions. Wohlfahrt et al. (2004) however suggest a cooling of the atmosphere already in autumn. One important factor influencing the differing results is that we define our seasons on an astronomical basis (Timm et al. 2008). Analyses by Wohlfahrt et al. (2004) for instance followed the PMIP-setup with the date of the vernal equinox fixed on 21 March. Seasonal values based on this method underestimate changes in the Northern Hemisphere in autumn (Braconnot et al. 2007a) which amounts to 0.9 °C according to our data processed with the PMIP-method (Figure 2.2b).

The atmosphere-vegetation feedback in our model is weaker than in previous studies (Gallimore et al. 2005; Wohlfahrt et al. 2004). In general, this feedback on temperature is induced by a northward shift of forest due to warmer mid-Holocene summer and autumn and it can be expected to be strongest in spring time through the snow masking of forest. Both the AOV-model (1.4 x 10^6 km^2, $\geq$ 60°N, see Figure 2.3) and the AV-model (1.2 x 10^6 km^2, $\geq$ 60°N) show a considerable northward extention in forest for mid-Holocene which is in general agreement with previous results (Wohlfahrt et al. 2008) and reconstructions (Bigelow et al. 2003). Despite this shift of forest, the atmosphere-vegetation feedback counteracts the insolation reduction in spring only marginally. During this season the change in forest leads to a reduction in albedo with

on average of 0.02 ($\geq$ 60°N) which is due to the snow masking of trees. This area shows a warming between 0.4 – 1.3 °C, other regions with no change in land cover (e.g. Greenland) show cooling (not shown). The mean over the whole area results in such a weak warming. This result corroborates the conclusions of the PMIP2 study (Braconnot et al. 2007b), that the magnitude of the atmosphere-vegetation feedback is smaller than previously discussed.
Concerning the atmosphere-ocean feedbacks including the sea ice-albedo feeback, the mid-Holocene simulations show less sea-ice cover compared to the pre-industrial simulations (see Figure 2.4), which is in agreement with previous studies (Ganopolski et al. 1998; Braconnot et al. 2007b). The orbitally induced increase in solar radiation during summer and autumn melts more sea-ice and warms up the ocean more strongly than in the pre-industrial climate. During autumn and winter, the ocean releases this heat to the atmosphere, resulting in higher air-temperatures compared to pre-industrial autumn and winter.
The positive taiga-tundra feedback and the positive sea ice-albedo feedback may strongly reinforce each other as both work at high northern latitudes. Despite the weak atmosphere-vegetation feedback, our simulations feature some positive synergistic effect between the atmosphere-ocean and atmosphere-vegetation feedback. However, the magnitude is smaller than simulated by Ganopolski et al. (1998) and Wohlfahrt et al. (2004). This corroborates results obtained with the EMIC MoBidiC for 9 ka (Crucifix et al. 2002). They suggest that a key point for this low synergy may be the differing sea-ice sensitivities between models. Another explanation for our ocean model with higher resolution may be that the main changes in sea-ice and forest cover occur spatially separated.

2.5 Summary of Chapter 2

We determine the response of climate to mid-Holocene insolation and the impact of atmosphere-ocean and atmosphere-vegetation feedbacks and their synergy on the northern latitude climate. Our model reproduces the basic picture of differences between the pre-industrial and mid-Holocene climate obtained from previous model studies but relates these changes to the components of the climate system in quite a different way. It simulates the mid-Holocene climate as follows: The direct atmospheric response to the orbital forcing is the most important cause of summer and autumn warming in the northern latitudes. The spring cooling is amplified by the atmosphere-ocean feedback most strongest. In autumn, the ocean duplicates the atmospheric warming and in winter, the ocean plays the most important role for the warming in this region. The contribution to the temperature signal from atmosphere-vegetation feedbacks is marginal and leads to a weak synergy between the atmosphere-vegetation and atmosphere-ocean feedback. To summarise, the warming of the northern latitudes during mid-Holocene can only be understood if all components of the Earth system model are taken into account. The atmosphere only explains a marginal warming of 0.05 °C annual mean

temperature. The contribution of the atmosphere-ocean and atmosphere-vegetation feedback and their synergy, however, lead to an additional warming of 0.39 °C. The most important modification of the orbital forcing can be related to the atmosphere-ocean interactions, likely as a consequence of its thermal inertia and the sea-ice albedo feedback. However, it should be kept in mind that feedbacks and their synergy are persumably strongly influenced by climate variability (Rimbu et al. 2004). Thus, the magnitude of the feedbacks may depend on the length of the analysis period.

Chapter 3

Climate variability-induced uncertainty in mid-Holocene atmosphere-ocean-vegetation feedbacks

3.1 Introduction

The mid-Holocene climate, 6000 years before present, is of particular interest to the understanding of the Earth System and abundant palaeoclimatic proxy records cover this period. Some boundary conditions of the climate system can be constrained accurately, in particular the variations in the Earth's orbit. These led to an increase of insolation during summer and the beginning of autumn, and to a decrease during winter compared to present day. The impact of this change in insolation on northern latitude climates has been intensively studied, e.g. by Wohlfahrt et al. (2004); Braconnot et al. (2007a); Otto et al. (2009b). It has been shown that both ocean and vegetation feedbacks as well as their synergy modify the seasonal climate response to mid-Holocene insolation considerably. However, there is no agreement on the relative magnitude of the two high-latitude feedbacks, and the strength of the synergy between them. Thus, we perform several sets of simulations with a General Circulation Model (GCM) to investigate, if this discrepancy is related to internal model variability, which may affect the magnitude of the estimated feedbacks.

Previous studies on the impact of feedbacks on mid-Holocene climate have been performed with Earth system Models of Intermediate Complexity (EMICs) and GCMs. A study with the EMIC CLIMBER-2 showed that the synergy between the atmosphere-ocean and atmosphere-vegetation feedback leads to an annual mid-Holocene warming (Ganopolski et al. 1998). Studies with GCMs either indicate a strong atmosphere-vegetation feedback (Wohlfahrt et al. 2004; Gallimore et al. 2005) or that the most important modification of the climate response is related to the atmosphere-ocean feedback (Otto et al. (2009b)) at the high latitudes. These divergent results may be ascribed to differences in the structure and parametrisation of the models as well as to the setup of the simulations. On the other hand, models exhibit internal variability due to non-linearities in the model physics and dynamics (Murphy et al. 2004). Therefore, the question arises how much of the differences among the models can be attributed to

sampling variability. Commonly, experiments are spun up until the climate trends are small, then the last 100 to 200 years are analysed (Braconnot et al. 2007a). Analysing a period of this length may not account for long-term climate variability, thus introducing uncertainty in the diagnosed feedbacks. To estimate this statistical uncertainty caused by the model's internal variability, we prolonged the simulations and repeated the factor-separation technique of the existing mid-Holocene feedback study by Otto et al. (2009b) five times.

3.2 Setup of Model Experiments

We performed several sets of simulations with the atmosphere-ocean GCM ECHAM5-MPIOM (Jungclaus et al. 2006) including the land surface scheme JSBACH (Raddatz et al. 2007) with a dynamic vegetation module (Brovkin et al. 2009). The experimental setup was designed to follow the factor-separation technique by Stein and Alpert (1993). For this reason, we performed four pre-industrial climate simulations, *0*kAOV, *0*kAO, *0*kAV, *0*kA and four mid-Holocene climate simulations, *6*kAOV, *6*kAO, *6*kAV, *6*kA. The capital letters indicate the components which are run interactively (A=atmosphere, O=ocean, V=vegetation). More details about the simulations are given in Otto et al. (2009b).
We calculated the contribution of each Earth system component to the mid-Holocene climate as follows:

$$\Delta AOV = 6kAOV - 0kAOV \tag{3.1}$$

$$\Delta A = (6kA - 0kA) \tag{3.2}$$

$$\Delta V = (6kAV - 0kAV) - (6kA - 0kA) \tag{3.3}$$

$$\Delta O = (6kAO - 0kAO) - (6kA - 0kA) \tag{3.4}$$

$$\Delta S = \Delta AOV - \Delta A - \Delta O - \Delta V \tag{3.5}$$

ΔAOV includes all feedbacks and synergistic effects. ΔA is the response of the atmosphere including snow cover, soil moisture and leaf phenology. The atmosphere-vegetation feedback ΔV is driven by the distribution of vegetation types and deserts. ΔO presents the atmosphere-ocean feedback including sea ice. ΔS describes the synergy between the atmosphere-vegetation and atmosphere-ocean feedback.
We prolonged the simulations in order to repeat the factor separation technique five times. The $0kAOV$ and $6kAOV$-simulations were run firstly for 1100 years, and the last 600 years were considered for the analysis. We divided these 600 years into five

analysis periods of 120 years each. The other six simulations were also prolonged up to 600 years and carried out in an analogous manner to the first analysis period (see Otto et al. (2009b)). To get a better picture of the the long-term climate variability caused by ocean dynamics, we ran the $0kAOV$ and $6kAOV$-simulations for further 1320 years.

3.3 Results and Discussion

This study confirms that the atmosphere-ocean feedback modifies the mid-Holocene temperature signal considerably. Figure 3.1 depicts the annual and seasonal mean 2m-temperature signal averaged over the five analysis periods with the uncertainty given as one standard deviation (δ) in ΔAOV, ΔA, ΔO, ΔV, ΔS of the five analysis periods. The simulations including all feedbacks and synergies, ΔAOV, show an annual warming in the mid-Holocene of 0.60°C (δ=0.11) north of 40°N. The seasonal mean air-temperature reveals an amplification of the seasonal cycle. In summer and autumn the warming reaches 1.27 °C (δ=0.06) and 1.91 °C (δ=0.08), respectively. Contrary to the insolation signal, the winter shows a warming of 0.64 °C (δ=0.17). Only the spring shows a cooling of -0.04 °C (δ=0.12) following the decrease of insolation. ΔA shows how much of the total climate response to the orbital-induced changes in insolation is ascribed to the direct atmospheric response. It shows a winter cooling of -0.16 °C (δ=0.02), a spring cooling of -0.19 °C (δ=0.04), a summer warming of 1.19 °C (δ=0.02), and an autumn warming of 0.76 °C (δ=0.01). The atmosphere-vegetation feedback ΔV is weak in all seasons. The boreal forest shifts poleward during the mid-Holocene, and through the snow-albedo feedback in spring, causes regionally an increase in temperature. Thus, only in spring ΔV leads to a slight warming of 0.08 °C (δ=0.06) counteracting the insolation changes. The atmosphere-ocean feedback ΔO shows the strongest modification of the direct climate response. It amplifies the autumn orbital signal by 1.06 °C (δ=0.17) and counteracts the cooling in winter by 0.73 °C (δ=0.27). The synergy between the atmosphere-ocean and atmosphere-vegetation feedback results in a slight warming in all seasons and leads to an annual warming of 0.08 °C (δ=0.12).

The uncertainty of the mean values is given by one standard deviation (Figure 3.1). The values of ΔA show similar results for each analysis period and are statistically robust (max. δ=0.04 in spring) because of the short-time memory of the atmosphere. Similarly, the weak springtime atmosphere-vegetation feedback ΔV occurs persistently in all five analysis periods (max. δ=0.06 in spring). By contrast, factors based on simulations with a dynamic ocean ($\Delta AOV, \Delta O, \Delta S$) show a large variability. This is due to the longer time scale of variations in the ocean compared to those in the atmosphere. The values of the atmosphere-ocean feedback ΔO and ΔAOV vary most between the analysis periods in comparison to the other factors. Their standard deviation is largest in winter (ΔO δ=0.27, ΔAOV δ=0.17). The large variability in the simulations with a dynamic ocean influences also the synergy term ΔS, so that the error bar exceeds the mean value of ΔS in all seasons, i.e. ΔS can change sign from one analysis period to

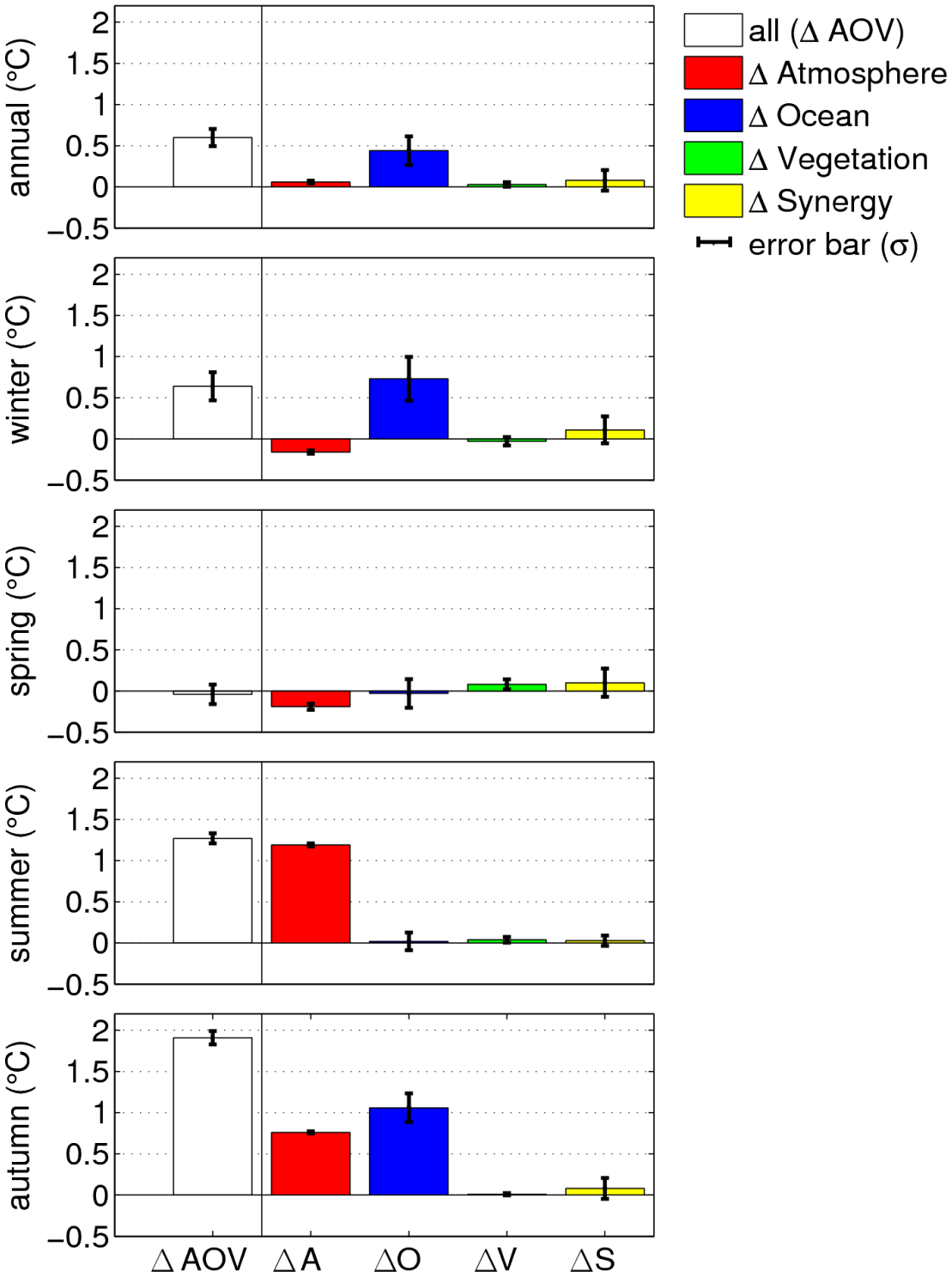

Figure 3.1: Contribution of factors to mean air-temperature (north of 40°) over five 120-year analysis periods. The error bar indicates one standard deviation. Please note that the length of the seasons differs between 0k and 6k, as we define the seasons by astronomical dates. Thus, the annual mean is not the linear average of the seasonal means.

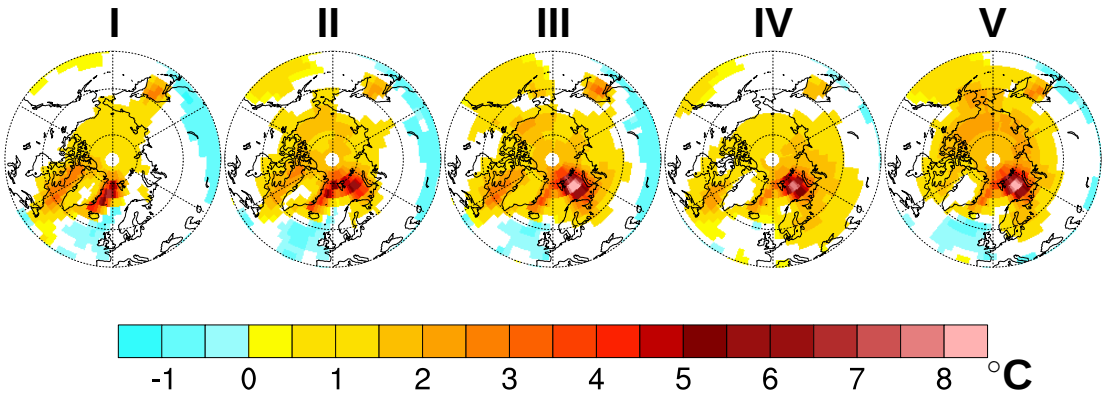

Figure 3.2: Winter mean temperature signal ΔAOV of the five analysis periods. Only significant values at the 99% level are displayed.

the other. This can be explained by the way the synergy term is calculated. It is the difference between ΔAOV (minuend) and the sum of the three components ΔA, ΔO and ΔV (subtrahend). ΔAOV and ΔO vary with a large amplitude and independently from each other as they are calculated from different simulations. Thus, the subtrahend can be larger than the minuend so that the synergy term becomes negative.

To analyse the large temperature variability of the simulations with a dynamic ocean more closely, we focus on the spatial temperature patterns of each analysis period. As the largest variability occurs in winter, Figure 3.2 depicts the spatial pattern of the winter mean temperature signal for ΔAOV. During the first two analysis periods the maximum temperature of ΔAOV occurs over the Greenland Sea with an anomaly of up to 6 °C. A weaker maximum appears around the Kamchatka Peninsula. From the second analysis period onwards, the maximum temperature anomaly appears in the Barents Sea region of up to 9 °C. The temperature maximum weakens slightly by 1 °C in the fourth but increases in the fifth analysis period. The winter mean temperature signals in the simulations with prescribed vegetation ΔAO (= 6kAO - 0kAO) are similar to ΔAOV (not shown).

To test the robustness of these winter temperature variability estimates, we extended the simulations $0kAOV$ and $6kAOV$ for 1320 years and calculated the standard deviation of the 120-year average winter temperature and sea-ice cover for sixteen analysis periods (Figure 3.3). The standard deviation of the air-temperature (Figure 3.3a) ranges from 0.2 to 2 °C . The largest variability with up to 2 °C appears in the Barents Sea as well around the Kamchatka Peninsula with up to 0.8 °C. The standard deviation of the fractional sea-ice cover (Figure 3.3b) is largest at the sea-ice margins and varies there from 0.01 to 0.1 in the Barents Sea. Figure 3.3 reveals that the regions of highest temperature variability match the areas of largest sea-ice variability. Furthermore, it shows that the patterns of variability with high values at the sea-ice margins are similar in 0k and 6k, and therefore statistically robust.

As the winter air-temperature variability is largest at the sea-ice margins, these regions

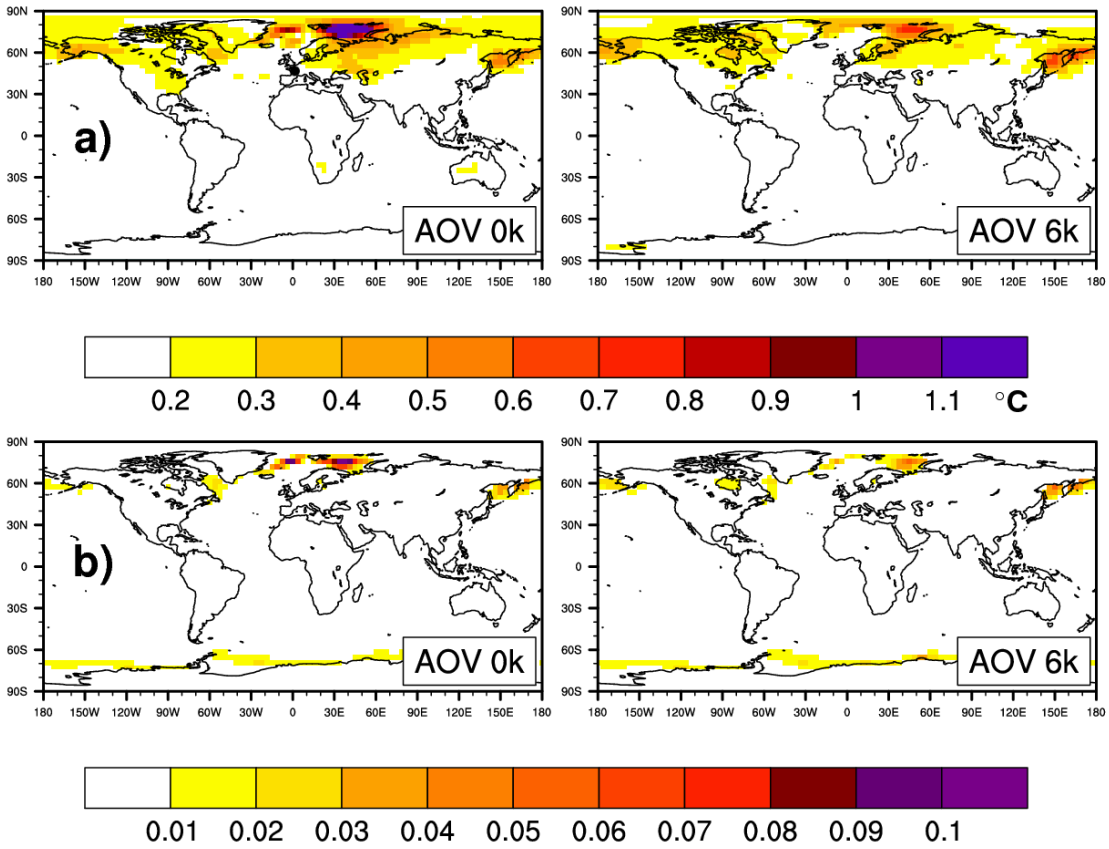

Figure 3.3: a) The standard deviation of 120-year mean winter air-temperature (n=16) for the pre-industrial and mid-Holocene AOV-simulation and b) the standard deviation of 120-year mean winter fractional sea-ice cover (n=16) for the pre-industrial and mid-Holocene AOV-simulation.

may be decisive for the long-term variations of the Northern Hemisphere temperature. To quantify the relation of these areas and the 120-year mean air-temperature north of 40°N, we selected three regions: two regions at the sea-ice margin – the Barents Sea and the region around the Kamchatka Peninsula – and the northern part of the North Atlantic (45°N - 60°N). We chose the latter region because it is only marginally influenced by sea-ice. In addition, the meridional overturning circulation is considered to have the potential to introduce long-term variations to the northern latitude climate (Ganachaud and Wunsch 2000). We correlated the average temperature of each region with the average temperature north of 40°N, excluding the particular region. In winter, the Barents Sea region (r=0.84 mid-Holocene, r=0.70 pre-industrial) and the region around the Kamchatka Peninsula (r=0.45 mid-Holocene, r=0.59 pre-industrial) are strongly correlated with the temperature north of 40°N. By contrast, the North Atlantic region shows a correlation coefficient close to zero in all seasons. Hence, in our model, the regions with the strongest temperature variability influence the average winter temperature north of 40°N decisively.

Our results reveal that internal climate variability affects the magnitude of the diagnosed feedbacks. This raises the question whether the variability generated in the model is comparable to natural variability. The internal variability integrated in the pre-industrial simulations ($0kAOV$, $0kAO$) compares reasonably well with the observed annual mean temperature variability from 1949-1998 (Delworth et al. 2002). The model reproduces the increased variability over continental extratropical regions. The simulated maximal variability emerges at the sea-ice margins, in particular over the Barents Sea, which is also in agreement with observations (Divine and Dick 2006). For this region, we find in our model the same strong coupling between local anomalies of atmospheric circulation and sea-ice cover (see Figure 3.4) as already analysed in previous modelling studies (Bengtsson et al. 2004; Koenigk et al. 2009). In summary, the variability generated in our model is comparable to observed variability and to the variability simulated by other models.

With our model, we are able to show that the statistical uncertainty affects the magnitude of the feedbacks. The question remains how much of the previous mid-Holocene results are affected by statistical uncertainty. The results from Ganopolski et al. (1998) with the EMIC CLIMBER-2 are statistically robust, as CLIMBER-2 does not generate climate variability (Petoukhov et al. 2000). Wohlfahrt et al. (2004) and Gallimore et al. (2005) performed their simulations with the GCMs IPSL and FOAM-LPJ, respectively. Wohlfahrt et al. (2004) based their analyses on 20-year averages. Gallimore et al. (2005) chose analysis periods of 100 and 400 years. As their analysis periods are about the same length or shorter than our 120-year analysis period, the estimated feedbacks may be affected by the statistical uncertainty. Furthermore, the studies by Wohlfahrt et al. (2004) and Gallimore et al. (2005) show a stronger vegetation feedback than our simulations. Possibly, their simulations could include a large vegetation variability. This could, in turn, enhance the ocean's variability. For example, Notaro and Liu (2007) showed with the GCM FOAM-LPJ that the variability in boreal forest significantly en-

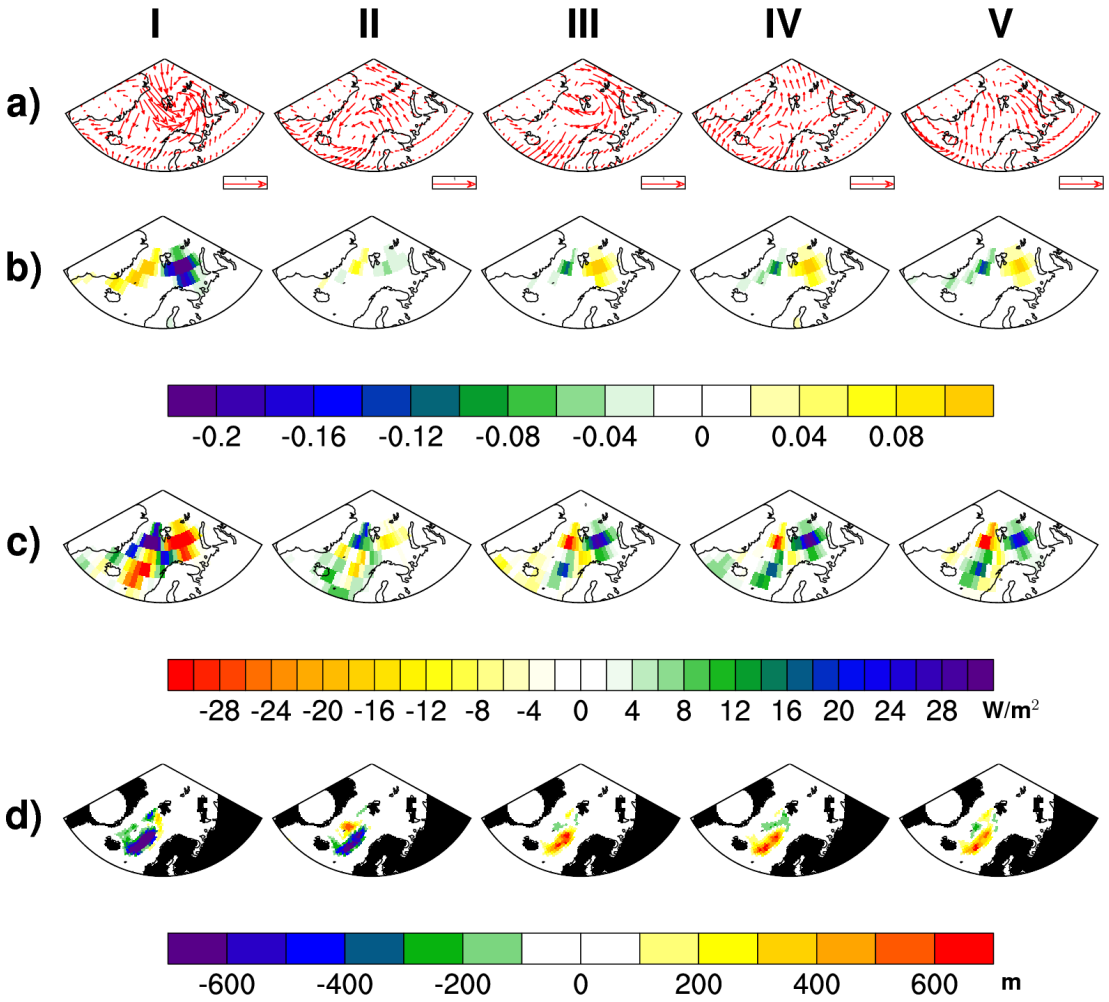

Figure 3.4: Differences between mean values of the five, consecutive 120-year periods and the 600 year mean value of the 0kAOV simulation in winter mean 10-m wind in m/s with a reference vector length of 1 m/s (a), winter mean sea-ice cover (b), winter mean ocean-atmosphere heat flux in W/m^2 (heat flux from the ocean to the atmosphere has a negative sign) (c), and ocean mixed layer thickness in m (d). Changes in the atmospheric circulation lead to variations in sea-ice cover in the Barents Sea. Anomalously high pressure over this region strengthens northerly winds and thus the sea ice transport into the Barents Sea. A low pressure anomaly, however, will maintain the westerly-to-southwesterly atmospheric flow into the region and thus the melting of sea ice. The heat flux to the atmosphere, the air-temperature and the mixed-layer thickness change, accordingly.

hances the variability in SSTs over the North Pacific. Thus, large vegetation variability may affect the magnitude of the synergy. Presumably, the discrepancy of the estimated feedbacks in different GCMs can be related, in part, to internal model variability.

3.4 Summary of Chapter 3

We have performed several sets of simulations to quantify how the statistical uncertainty affects the estimated atmosphere-vegetation and atmosphere-ocean feedback and their synergy to mid-Holocene insolation. Although the analysis period is long (120 years), it leads to statistical uncertainty which has different effects on the magnitude of the considered feedbacks. The atmosphere response and the weak atmosphere-vegetation feedback are statistically robust. By contrast, the factors derived from simulations with an interactive ocean are sensitive to long-term anomalies in sea-ice cover. As a result, GCM simulations with an interactive ocean should include a long spin-up time as well as a long analysis period to reduce the statistical uncertainty. This is also important with regard to model intercomparison studies. Nevertheless, this study confirms that the most important modification of the orbital forcing can be related to the atmosphere-ocean interactions. The divergent results of the previous mid-Holocene studies can therefore only partly be related to internal variability.

Chapter 4

Sensitivity of the atmosphere-vegetation feedback

4.1 Introduction

Palaeoclimate modelling provides an opportunity to examine the question of how different forcings and feedbacks have influenced the variability of the climate. In this respect, the mid-Holocene, around 6000 years before present, is suited as a test climate period. Changes in the Earth's orbit yield a small increase in annual mean insolation in the northern latitudes (2.5 W/m^2, north of 60°N). Despite this relative weak insolation forcing, palaeo-reconstructions (e.g. Davis et al. (2003); Kaplan et al. (2003)) suggest that the annual mean temperature of the northern latitudes was distinctly increased in comparison to pre-industrial climate. This warming of northern latitudes has been supported by climate model simulations (e.g. Ganopolski et al. (1998); Wohlfahrt et al. (2004); Gallimore et al. (2005); Otto et al. (2009b)).
Furthermore, these studies have shown that the climate response to mid-Holocene orbital forcing was considerably influenced by two main climate feedbacks: the atmosphere-ocean feedback (Hewitt and Mitchell (1998); Otto et al. (2009b,a)) and the atmosphere-vegetation feedback (Foley et al. 1994; Wohlfahrt et al. 2004). This conclusion appears to be robust across different kinds of models and a range of experimental designs. However, the studies differ in the relative magnitude of the feedbacks and the strength of the synergy between them.
This discrepancy may be ascribed to differences in the setup of simulations, model configurations or statistical uncertainty caused by internal model variability. The study by Otto et al. (2009a) showed that simulations with an interactive ocean reveal a large variability at sea-ice margins. This variability leads to a sampling error which affects the magnitude of the diagnosed feedbacks. However, this can only partly explain the divergent model results. Another explanation may be the difference in structure and parametrisation of the land surface in the climate models. Thus, we perform several sets of simulations with a General Circulation Model (GCM) to investigate how different land-surface parametrisations affect the mid-Holocene climate signal at the high northern latitudes.
The climate of the high northern latitudes is influenced strongly by albedo-related feed-

backs (Harvey 1988). For instance, a surface fully covered with fresh snow has a high albedo. However, the actual magnitude of the albedo of a snow-covered surface depends on the type of vegetation which covers the ground. Forest with its canopy and height protrudes the snow layer. From a bird's eye view, a snow-covered forest appears darker than low vegetation covered with snow or bare ground. Thus, snow-covered forest has a lower albedo than snow-covered grass (Otterman et al. 1984). Even forests without foliage like deciduous forest (Wang 2005) significantly reduce the albedo of snow-covered land (see Table 4.2). This is the basis for the positive atmosphere-vegetation feedback. A replacement of tundra by forest decreases the surface albedo during the cold season which leads to a warming and favours further growth of boreal forest.

Several model studies indicate that this positive atmosphere-vegetation feedback played an important role for the mid-Holocene climate. Foley et al. (1994) have performed a mid-Holocene simulation with the atmosphere-ocean GCM GENESIS with an imposed forest extension. In their study the increase in forest yields warming of approximately 4 °C north of 60°N during spring which counteracts the cooling by the seasonally decreased insolation due to orbital forcing. Wohlfahrt et al. (2004), using the coupled ocean-atmosphere GCM IPSL asynchronously coupled with the equilibrium vegetation model BIOME1, simulated a polward expansion of boreal forest cover and an expansion in mid-latitude grasslands during the mid-Holocene. The expanded forest, by masking snow cover, led to a springtime warming of 0.95 °C north of 40°N. Gallimore et al. (2005) performed simulations with the atmosphere-ocean GCM FOAM coupled to the dynamic vegetation model LPJ. Their simulations indicate a similar mid-Holocene vegetation distribution like Wohlfahrt et al. (2004) but result in a weaker springtime warming (circa 0.4 °C, north of 60°N). Diffenbaugh and Sloan (2002) prescribed mid-Holocene vegetation distribution from a plant fossil record to simulations with the GCM CCM-LSM. They found that the changes in vegetation cover can lead to differences between present-day and mid-Holocene climate which are of the same magnitude as the difference due to orbital forcing.

However, the simulated climate signal does not only depend on changes in vegetation cover, but also on differences in land-surface parametrisation. Bony et al. (2006) stated in a review article that the main source of errors in models arise from the way the albedo of snow is parameterised in models. The study by Qu and Hall (2007) compares 18 GCMs and reveals that the models vary in the strength of the snow-albedo feedback because of the various snow-albedo parametrisations. Models with the most complex snow-albedo parametrisation show a significantly weaker snow-albedo feedback than observed. The snow-albedo parametrisation emerges not only as a critical factor controlling the snow-albedo feedback but also the global climate sensitivity. Levis et al. (2007) showed that their simulations with two equally justifiable snow-cover parametrisations, which directly affect the surface albedo in snow-covered regions, lead to a 0.2 °C difference in climate sensitivity. Roesch and Roeckner (2006) demonstrated how different parametrisations of the surface albedo and snow cover in two versions of the same climate system model differ from observations. Models tend to have larger

deficiencies in modelling snow at forest sites than at open sites, as an evaluation of snow-pack models with observations reveals (Rutter et al. 2009), possibly due to more complex snow processes at forest sites. Thus, the parametrisation of both albedo of snow and snow cover contribute considerably to the systematic uncertainty in the simulated atmosphere-vegetation feedback.
Consequently, the discrepancy between modelling results on mid-Holocene feedbacks may arise from different parametrisations of the albedo of snow. To test this hypothesis, we first investigate the atmosphere-vegetation feedback in detail to understand the processes which are involved in this feedback. Secondly, we investigate the sensitivity of the atmosphere-vegetation feedback with respect to the parametrisation of the albedo of snow-covered land. To evaluate how different parametrisations of the albedo of snow affect the strength of the atmosphere-vegetation feedback under mid-Holocene insolation forcing, we perform simulations with three different snow-albedo parametrisations: a) simulations with a snow-albedo parametrisation which includes a weak reduction of the albedo of snow by deciduous forest, b) simulations with a snow-albedo parametrisation which includes strong reduction of the albedo of snow by deciduous forest and by evergreen forest, c) simulations with a snow-albedo parametrisation which takes into account the aging of snow and includes strong reduction in the albedo of snow by evergreen forest. The aim of this study is to find reasons for the weaker atmosphere-vegetation feedback simulated with ECHAM5-JSBACH (Otto et al. 2009a,b) than suggested by previous modelling studies of the mid-Holocene.
The sections are organised as follows. In Section 4.2.1, the albedo schemes are presented and in Section 4.2.2, the setup of the experiments is described. The results of this chapter are divided into two parts. Section 4.3.1 contains the comparison of the utilised parametrisations of albedo of snow and Section 4.3.2 describes how these parametrisations impact the strength of the atmosphere-vegetation feedback under mid-Holocene conditions. In Section 4.4, the results are discussed.

4.2 Model and experimental setup

We perform the simulations with the GCM ECHAM5 (Roeckner et al. 2003), including the land surface scheme JSBACH (Raddatz et al. 2007) with a dynamic vegetation module (Brovkin et al. 2009). For this study, we use the same model, the same resolution and a similar experiment setup as described in Otto et al. (2009b) and Otto et al. (2009a). However, due to changes in the operating system of the supercomputer, we had to use a newer version of the model. Nevertheless, the results of this chapter can be compared directly with the results of the studies presented in Otto et al. (2009b) and in Otto et al. (2009a)

4.2.1 Albedo scheme

The land-surface processes are in all simulations calculated by JSBACH. The albedo scheme in JSBACH computes the temporal and spatial changes of the land-surface albedo. It provides a spatially explicit surface albedo calculation for the near infrared (NIR) as well as for the visible range (VIS). For the snow-free land, JSBACH follows a similar approach as described in Rechid et al. (2008) with a temporal variation of surface albedo as a function of vegetation phenology derived from satellite data with the sensor Moderate-Resolution Imaging Spectroradiometer (MODIS) (Schaaf et al. 2002). In general, the albedo is calculated separately for surfaces covered by green leaves and for the underlying surface of the soil. If the land surface, however, is snow covered, the albedo of a snow-covered fraction of the grid box is additionally computed similar to the parametrisation in ECHAM5 (Roeckner et al. 2003). For forest, an albedo value of $\alpha_F = 0.25$ is set for the part of the canopy covered with snow. In contrast, the vegetation types of grass and shrubs are assumed to be completely covered by snow, so that the same albedo value is used for these areas as for snow-covered bare land. This albedo of snow is assumed to decrease linearly with surface temperature, ranging from a minimum value at melting point ($\alpha_{VIS} = 0.5$, $\alpha_{NIR} = 0.3$) to a maximum value for temperatures of less than -5 °C ($\alpha_{VIS} = 0.9$, $\alpha_{NIR} = 0.7$) (Roesch and Roeckner 2006). We refer to this model as the model with standard parametrisation.
For another set of simulations, we change the parametrisation of how forest reduces the albedo of snow. In the model with standard parametrisation, deciduous forest has only a weak effect on the albedo of snow because of the loss of its foliage during the cold season. It is assumed that only evergreen forest with remaining leafs can effectively mask the albedo of snow. Roesch and Roeckner (2006), however, described this as a deficiency and suggest the introduction of a stem area index for deciduous trees. When deciduous trees have lost their needles or leaves, this stem area index mimics the stem and branches shadowing the ground below the canopy. In the model with standard parametrisation, this stem area index is set to 1 which introduces a weak snow masking for deciduous forest (Figure 4.1). However, both field measurements (e.g. Betts and Ball (1997)) and satellite analysis (e.g. Wang (2005); Moody et al. (2007)) reveal that deciduous forest can also mask snow effectively and reduces the albedo of snow up to 0.3 (see Table 4.2). Accordingly, we increase the strength of how forest masks the albedo of snow in JSBACH. To account for a stronger snow masking by deciduous forest, we set the stem area index to 3. In addition, we introduce a stronger snow masking by evergreen forest by reducing the albedo of snow-covered canopy from $\alpha_F = 0.25$ to $\alpha_F = 0.20$ (Sturm et al. 2005). To simulate a similar control climate like in the model with standard parametrisation, we increased the minimum albedo of snow in the near infrared from $\alpha_{NIR} = 0.3$ to $\alpha_{NIR} = 0.4$. We refer to this parametrisation as the model with strong snow masking.
Another process affecting the albedo of snow is the metamorphism of snow with time. The albedo of snow changes with the age of snow due to changes in the size of snow grain,

experiment name	*prescribed vegetation cover*	*duration [years]*	*parameters changed*
ΔV			
$6kAV$	–	480	–
$0kAV$	–	480	–
$6kA$	from $0kAV$	250	–
$0kA$	from $0kAV$	250	–
ΔVse			
$6kAVsm$	–	480	snow masking of deciduous trees and evergreen forest
$0kAVsm$	–	480	snow masking of deciduous trees and evergreen forest
$6kAsm$	from $0kAVse$	250	snow masking of deciduous trees and evergreen forest
$0kAsm$	from $0kAVse$	250	snow masking of deciduous trees and evergreen forest
ΔVsa			
$6kAVsa$	–	480	snow masking of evergreen forest snow melting
$0kAVsa$	–	480	snow masking of evergreen forest snow melting
$6kAsa$	from $0kAVsa$	250	snow masking of evergreen forest snow melting
$0kAsa$	from $0kAVsa$	250	snow masking of evergreen forest snow melting

Table 4.1: List of simulations.

impurities in the snow and the presence of liquid water in the snow. Thus, the majority of GCMs calculate the albedo of snow with a dependence on snow age (Levis et al. 2007; Qu and Hall 2007). In the model with standard parametrisation, the albedo of snow is calculated with an explicit temperature dependence. To change this calculation to a dependence on snow age, the snow albedo parametrisation of the Biosphere Atmosphere Transfer Scheme (BATS) (Dickinson et al. 1986) was implemented in the albedo scheme of JSBACH [1]. In this parametrisation, the albedo of snow depends on temperature in a prognostic way. A snow-aging factor is introduced which takes the age of snow into account in an empirical way. Similar to the model with strong snow masking, the albedo of snow-covered canopy is reduced from $\alpha_F = 0.25$ to $\alpha_F = 0.20$. This parametrisation is called the snow-aging model in the following. The implemented snow-albedo scheme of BATS is described in more detail in the Appendix A.

[1] This was done by Dr. Thomas Raddatz.

4.2.2 Simulation protocol

In total, we performed 13 simulations (see Table 4.1): four simulations with the model with standard parametrisation, four simulations with the model with strong snow masking, four simulations with the snow-aging model. All simulations were run with atmospheric CO_2-concentrations set to 280 ppm and with the same sea-surface temperature and sea-ice cover prescribed as monthly values. The last 240 years of all experiments were considered for the analysis.
Four simulations with the model with standard parametrisation are required to calculate the pure contribution of the atmosphere-vegetation feedback ΔV to the mid-Holocene climate signal: two simulations with dynamic vegetation run for 480 years, one with pre-industrial ($0kAV$) and one with respective mid-Holocene orbital forcing ($6kAV$). The two corresponding atmosphere-only simulations had the vegetation prescribed from the $0kAV$-simulation and were run for 250 years with pre-industrial ($0kA$) and respective mid-Holocene orbital forcing ($6kA$). To calculate the pure contribution of the atmosphere-vegetation feedback ΔV, we have to compare the results of the two simulations with the vegetation run interactively ($\Delta AV = 6kAV$ - $0kAV$) with the two atmosphere-only simulations ($\Delta A = 6kA - 0kA$):

$$\Delta V = (6kAV - 0kAV) - (6kA - 0kA) \tag{4.1}$$

The pure contribution ΔV can be evaluated for all climate parameters. If we consider a specific climate parameter, for example the air temperature [T], we use the symbol $\Delta V[T]$.
The four simulations with the model with strong snow masking and the four simulations with the snow-aging model were performed similarly. The simulations with the model with strong snow masking are labelled as follows: $0kAVsm$, $6kAVsm$, $0kAsm$, $6kAsm$. The vegetation distribution of the atmosphere-only simulations ($\Delta Asm = 6kAsm - 0kAsm$) was prescribed from the $0kAVsm$ simulation. The simulations with the snow-aging model are referred to as: $0kAVsa$, $6kAVsa$, $0kAsa$, $6kAsa$. The atmosphere-only simulations ($\Delta Asa = 6kAsa - 0kAsa$) run with prescribed vegetation of the $0kAVsa$ simulation. We calculate the corresponding our contribution by the atmosphere-vegetation feedback as in equation 4.1.

$$\Delta Vsm = (6kAVsm - 0kAVsm) - (6kAsm - 0kAsm) \tag{4.2}$$

$$\Delta Vsa = (6kAVsa - 0kAVsa) - (6kAsa - 0kAsa) \tag{4.3}$$

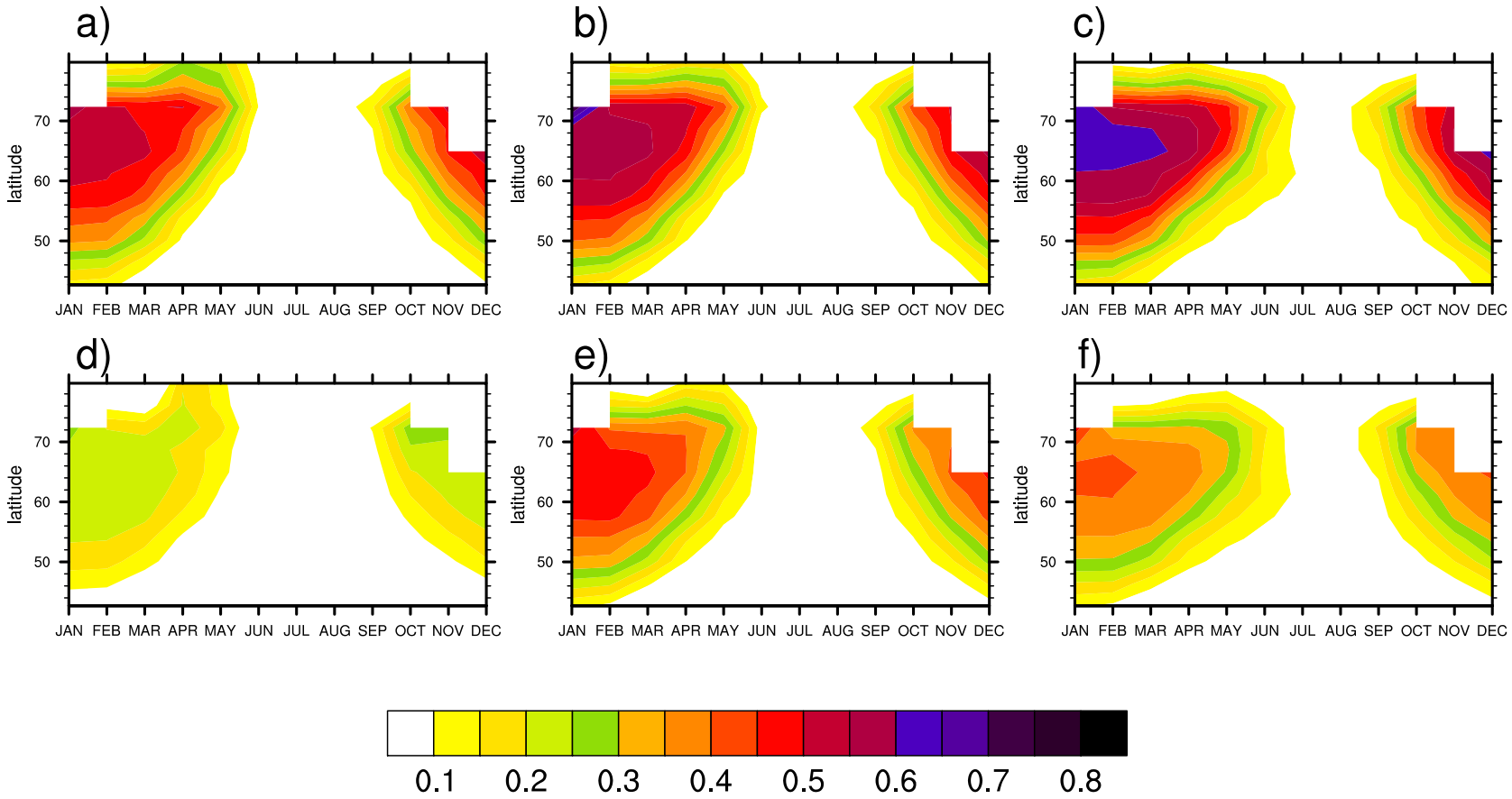

Figure 4.1: Shown is the difference between grass-albedo (VIS+NIR) and forest-albedo (VIS+NIR). We refer to this difference as strength of snow-masking because large changes occur only when the surface is covered by snow. The seasonal cycle of the strength of the snow-masking is shown as the zonal mean north of 40°N for the model with standard parametrisation (a,d), the model with strong snow masking (b,e) and the snow-aging model (c,f) for each forest type evergreen forest (upper row) and deciduous forest (lower row).

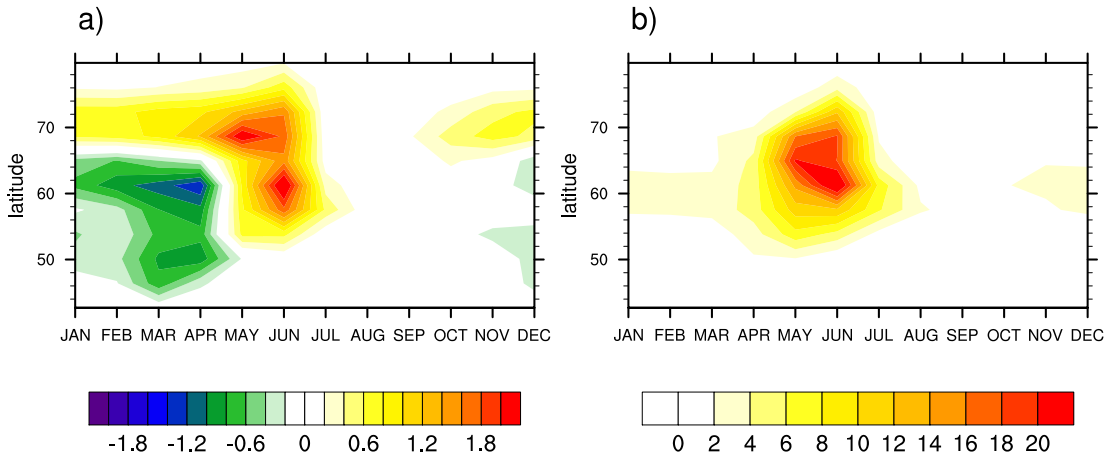

Figure 4.2: Anomalies of snow depth in mm for the model with strong snow masking $0kAVsm$ (a) and the snow-aging model $0kAVsa$ (b) relative to the model with standard parametrisation $0kAV$. Please note the different scale of the label bars.

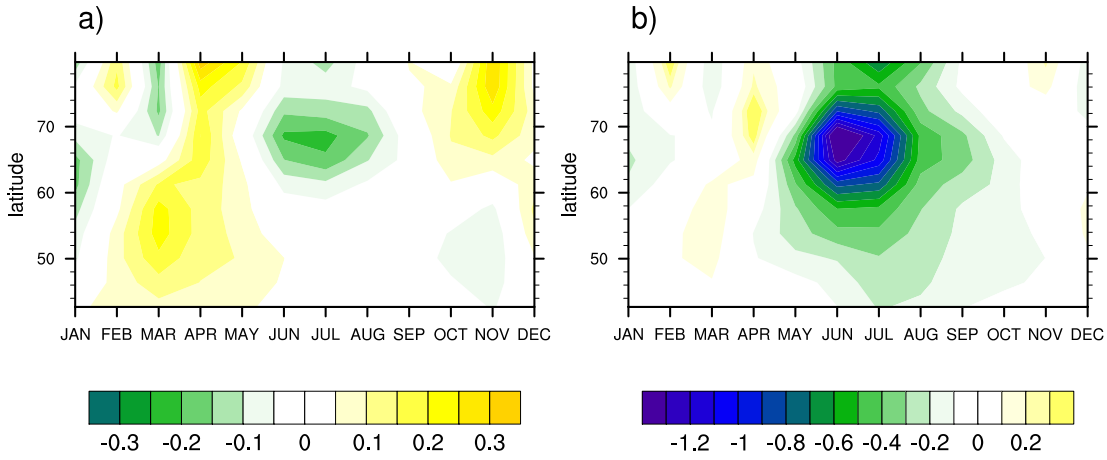

Figure 4.3: Anomalies of air-temperature in °C for the model with strong snow masking $0kAVsm$ (a) and the snow-aging model $0kAVsa$ (b) relative to the model with standard parametrisation $0kAV$. Please note the different scale of the label bars.

	model with standard parametrisation	*model with strong snow masking*	*snow-aging model*	*measurements*	*type of measurements*	*reference*
grass - evergreen	0.1 - 0.6	0.1 - 0.6	0.1 - 0.7	0.5 - 0.6	three sites	Essery et al. (2009)
				0.3	satellite	Moody et al. (2007)
				0.1 - 0.5	satellite	Barlage et al. (2005)
				0.2	satellite	Jin et al. (2002)
				0.6	ten sites	Betts and Ball (1997)
grass - deciduous	0.1 - 0.3	0.1 - 0.5	0.1 - 0.4	–	three sites	Essery et al. (2009)
				0.3	satellite	Moody et al. (2007)
				0.1 - 0.5	satellite	Barlage et al. (2005)
				0.1 - 0.3	satellite	Jin et al. (2002)
				0.5	ten sites	Betts and Ball (1997)

Table 4.2: Strength of snow masking of the three models: model with standard parametrisation, model with strong snow masking and snow-aging model, compared with different measurements.

4.3 Results

4.3.1 Comparison of parametrisations

The three different parametrisations of the snow-covered surface yield different values of the albedo of snow-covered grass and forest. Figure 4.1 shows the seasonal cycle of the zonally-averaged difference between the albedo of grass and the albedo of forest. As large differences occur only when the surface is covered by snow, we refer to this difference as the strength of snow masking.
In the model with standard parametrisation (Figure 4.1a), the strength of snow masking of evergreen forest ranges from 0.1 to 0.6 with the strongest effect in the region between 60-70°N. The strength of snow masking decreases during spring and vanishes late in May when the snow has completely melted. At the beginning of September, with the start of the cold season in the high northern latitudes, the snow masking begins and increases with time. The snow masking of deciduous forest is much weaker than of evergreen forest (Figure 4.1d). The strength of snow masking varies only between 0.1 and 0.3. The annual cycle of the strength of snow masking is similar to the one of evergreen trees.
The model with strong snow masking reveals a larger annual cycle for the strength of snow masking (Figure 4.1b,e) compared to the model with standard parametrisation. The snow masking of deciduous forest is increased by almost factor two due to the increase in the stem-area index. The strength ranges from 0.1 to 0.5 and is strongest in the region between 55-70°N. The strength of snow masking of evergreen trees is similar to the one of the model with standard parametrisation. However, the region with the strongest snow masking reaches further south up to 55°N as opposed to the model with standard parametrisation.
The parametrisation of the snow albedo depending on a snow-aging factor leads also to an increase in the strength of the snow masking (Figure 4.1c,f) compared to the model with standard parametrisation. The strength of the snow masking of deciduous forest ranges from 0.1 to 0.4. Thus, this parametrisation yields a less pronounced increase in the strength of snow masking of deciduous forest compared to the model with strong snow masking. The strength of snow masking by evergreen forest, however, increases by 0.05 compared to the two other parametrisations. For both forest types the snow masking persists longer in the course of the year than in the model with standard parametrisation. This indicates that the snow melt is delayed by approximately one month compared to the other two model configurations. Figure 4.2 reveals that in May, the snow depth is on average 20 mm higher than in the model with standard parametrisation.
The reasons for the enhanced snow masking and the delayed snow melt can be attributed to the way the albedo of snow is parametrised in the snow-aging model. Firstly, the albedo of a snow-covered canopy (α_F) is reduced by 0.05 compared to the model with standard parametrisation which increases the difference between snow-

covered grass and forest. This affects the snow masking of evergreen forest. Secondly, the maximum and minimum values of the albedo of snow differ in snow-aging model compared to the model with standard parametrisation. Snow in the snow-aging model can have a higher maximum albedo ($\alpha_{VIS} = 0.95$) in the visible range compared to in the model with standard parametrisation ($\alpha_{VIS} = 0.90$). The minimum albedo of snow is crucial for the snow melt. In the snow-aging model, the calculation of the minimum albedo of snow depends on the snow-age factor and decays exponentially (see Appendix A). If snow falls, it is assumed that fresh snow is rather white and therefore the albedo of snow is set to a high albedo value (max. $\alpha_{VIS} = 0.95$). In contrast, the minimum albedo of the model with standard parametrisation is linearly reached when the temperature is at the melting point. The albedo of snow is in this parametrisation independent of the age of snow, so that as soon as the temperature exceeds freezing the minimum albedo value of snow is used ($\alpha_{VIS} = 0.5$). Thus, the parametrisation with the snow-aging factor delays the snow melt compared to the model with standard parametrisation (Figure 4.2). This delay results in cooler mean summer temperature up to 1.5 °C in the regions which are periodically snow-covered (Figure 4.3).
The albedo of snow can be measured by aircraft and satellite, remote sensing and ground observations (Table 4.2). These measurements have shown that the albedo of snow is strongly variable and depends on various factors like e.g. the type of snow (Moody et al. 2007). Thus, the estimates for the strength of the snow masking vary between 0.1 and 0.6 for evergreen forest and between 0.1 and 0.5 for deciduous forest. However, the studies listed in Table 4.2 consistently show that the strength the of snow masking by evergreen forest is only slightly stronger than the strength of the snow masking of deciduous forest. In general, in all three models the strength of the snow masking is within the range of the observed snow masking. Nevertheless, the strength of the snow masking of deciduous forest in the model with standard parametrisation is at the low end of the range of observations, the strength of the snow masking of evergreen forest in the snow-aging model is at the high end of the range of observations.

4.3.2 Atmosphere-vegetation feedback

To assess how the different snow-albedo parametrisations influence the strength of the atmosphere-vegetation feedback under mid-Holocene forcing, we performed several sets of simulations (see Section 4.2.2) using the model with standard parametrisation, the model with strong snow-masking and the snow-aging model. The basis for the mid-Holocene atmosphere-vegetation feedback is the northward shift of forest compared to the pre-industrial situation (Claussen 2004). The change in forest of the standard, snow-masking and snow-aging model is depicted in Figure 4.4 and Table 4.3. All three parametrisations produce an expansion of forest compared to the pre-industrial climate. The largest increase for the region north of 60°N simulates the model with strong snow masking with 12.71 x 10^5 km^2 followed by the model with standard parametrisation with an increase of 11.29 x 10^5 km^2. The weakest forest growth is produced by the

	model with standard parametrisation	model with strong snow masking	snow-aging model
change in area covered by vegetation and desert in 10^5 km^2			
evergreen forest	4.84	6.82	4.89
deciduous forest	6.45	5.89	4.36
grass	-1.68	-1.96	1.85
shrubs	-0.46	0.03	1.06
desert fraction	-9.15	-10.78	-12.16
change in temperature	$\Delta V[T]$	$\Delta Vsm[T]$	$\Delta Vsa[T]$
annual	0.07	0.20	0.16
winter	0.03	0.12	0.07
spring	0.12	0.34	0.37
summer	0.10	0.24	0.15
autumn	0.04	0.10	0.05
climate change in spring	ΔV	ΔVsm	ΔVsa
surface albedo	-0.02	-0.03	-0.02
precipitation $mm/season$	0.28	0.85	2.48
snow depth in mm	-0.53	-1.70	-0.96
sensible heat flux in W/m^2	-0.42	-0.72	-0.30
latent heat flux in W/m^2	-0.38	-0.69	-0.76
net surface solar radiation W/m^2	1.05	1.77	1.40
net surface thermal radiation in W/m^2	-0.04	0.00	-0.03
cloud cover fraction	0.002	0.004	0.003

Table 4.3: Summary of the atmosphere-vegetation feedbacks of the three models (model with standard parametrisation = ΔV, model with strong snow masking = ΔVsm, snow-aging model = ΔVsa). All values are spring mean values and averaged over land over the area 60°-90°N. The change in vegetation cover is derived from the simulations with dynamic vegetation. Please note that fluxes towards the atmosphere (sensible and latent heat fluxes) are negative.

snow-aging model with 9.25 x 10^5 km^2. The forest expansion comprises the increase in evergreen and deciduous forest. Evergreen forest increases only north of 60°N in Northern Europe, North-Western Siberia as well as in Northern Canada. Deciduous forest, however, increases mainly in North-Eastern Siberia but reaches further south up to 50°N. The patterns of vegetation cover are similar for all parametrisations. Nevertheless, the largest increase in evergreen forest averaged over the area north of 60°N is simulated by the model with strong snow masking with 6.82 x 10^5 km^2, the largest increase in deciduous forest is produced by the model with standard parametrisation with 6.45 x 10^5 km^2. In the model with standard parametrisation and in the model with strong snow masking, the forest grows more at the expense of grass and shrubs than in the snow-aging model (Table 4.3). In the snow-aging model, the forest increases more at the expense of cold desert (Table 4.3) than with the other two parametrisations.
Figure 4.5 depicts the mean seasonal air-temperature response to the change in insolation averaged over the region north of 60°N. The temperature response is divided into the pure response of the atmosphere and the pure contribution of the atmosphere-vegetation feedback to the temperature signal. All three parametrisations follow the orbital-induced change in insolation in the temperature signal ($\Delta A, \Delta Asm$ and ΔAsa). The mid-Holocene decrease in insolation during winter and spring, compared to present day, results in a decrease in temperature in winter (ΔA =-0.08, ΔAsm =-0.13, ΔAsa =-0.02) and spring (ΔA =-0.07, ΔAsm =-0.09, ΔAsa = -0.22). The enhanced insolation during summer and the beginning of autumn yields an increase in temperature in summer ($\Delta A = 1.73$, $\Delta Asm = 1.73$, $\Delta Asa = 1.67$) and autumn ($\Delta A = 0.95$, $\Delta Asm = 0.92$, $\Delta Asa = 0.95$) compared to pre-industrial climate. The magnitude of the atmosphere signal varies between the three parametrisations. This is due to the changes in the snow-albedo scheme, which results in slightly diverging pre-industrial climates of the atmosphere-vegetation simulations as shown in Section 4.3.1 and Figure 4.3. Hence the different parametrisations produce a diverging climate response to the mid-Holocene insolation forcing as well. The temperature anomaly compared to the model with standard parametrisation is larger in the snow-aging model (maximum in spring of -0.15 °C) compared to the model with strong snow masking (maximum in winter of -0.05 °C).
The pure contribution of the atmosphere-vegetation feedback (Figure 4.5 and Table 4.3) contributes a warming to the mid-Holocene climate signal throughout the year. In summer and in autumn, the atmosphere-vegetation feedback amplifies the warming of the direct atmospheric signal. In both seasons, thepure contribution of the atmosphere-vegetation feedback is largest in the model with strong snow masking with 0.24 °C in summer and 0.10 °C in autumn. In winter and spring, the atmosphere-vegetation feedback contributes a warming which counteracts the cooling of the atmospheric signal. The contribution of warming is stronger in spring than in winter. In the model with standard parametrisation, the $\Delta V[T]$ reaches 0.12 °C in spring. The $\Delta Vsm[T]$ and $\Delta Vsa[T]$ counteract the cooling more strongly by about a factor of three. The model with strong snow masking produces a temperature anomaly of 0.34 °C in spring. The

pure contribution of the atmosphere-vegetation feedback is slightly larger with 0.37 °C in the snow-aging model compared to the model with strong snow masking.

As the largest temperature increase caused by the pure contribution of the atmosphere-vegetation feedback occurs in spring (Figure 4.5), we focus on the spring season to analyse how the atmosphere-vegetation feedback works. The spatial distribution of the spring air-temperature is shown in Figure 4.6. The positive temperature anomaly is largest in the circum-polar belt between 60-70°N. The temperature increases up to 0.6 °C in the model with standard parametrisation. The temperature rise of the model with strong snow masking is stronger than in the model with standard parametrisation. In North-Eastern Siberia, the temperature rises up to 1.3 °C. This is the region where deciduous forest expands. The implemented stronger snow-masking of deciduous forest in the model with strong snow masking results in a stronger temperature increase compared to in the model with standard parametrisation. The temperature pattern of the snow-aging model looks similar to the model with standard parametrisation but with a more pronounced temperature rise by up to 0.3 °C. The temperature increases particularly in the regions of evergreen forest growth. This is due to the stronger snow-masking of evergreen forest in the snow-aging model compared to the standard parametrisation (see Figure 4.1).

The different model configurations, however, reveal not only patterns of warming but also patterns of cooling. The standard and the snow-masking model show cooling patterns over Northern Europe and Southern Canada of up to -0.4 °C. The cooling is somewhat stronger in the model with strong snow masking than in the model with standard parametrisation. These cooling patterns are marginally present in the snow-aging model.

To analyse the temperature change caused by the pure contribution of the atmosphere-vegetation feedback more closely, we examine the surface energy budget. The temperature signal is strongly affected by the available solar energy at the surface. This energy is absorbed by the Earth's surface and eventually transferred back into the atmosphere by thermal radiation, by latent heat flux and by sensible heat flux. The signal in net surface solar radiation is shown in Figure 4.7. In the regions of forest expansion the net surface solar radiation increases compared to present-day climate by 2 – 12 W/m^2. Nevertheless, the patterns of net surface solar radiation show regions with a decrease in net surface solar radiation. The net surface solar radiation decreases over North America between 40-60°N and North-East Europe by about -4 W/m^2 compared to the pre-industrial signal. These patterns of decrease are similar to the patterns of decrease in the temperature signal (Figure 4.6).

The magnitude of the net solar surface radiation depends on the surface albedo. In spring, all three parametrisations show a reduction in surface albedo compared to present-day climate (Figure 4.8). The decrease ranges from -0.14 to -0.06 and follows the pattern of increased forest (Figure 4.4). The strongest decrease is obtained with the model with strong snow masking. This model simulates a reduction of up to -0.20 regionally in North-Eastern Siberia. This could be expected since this model

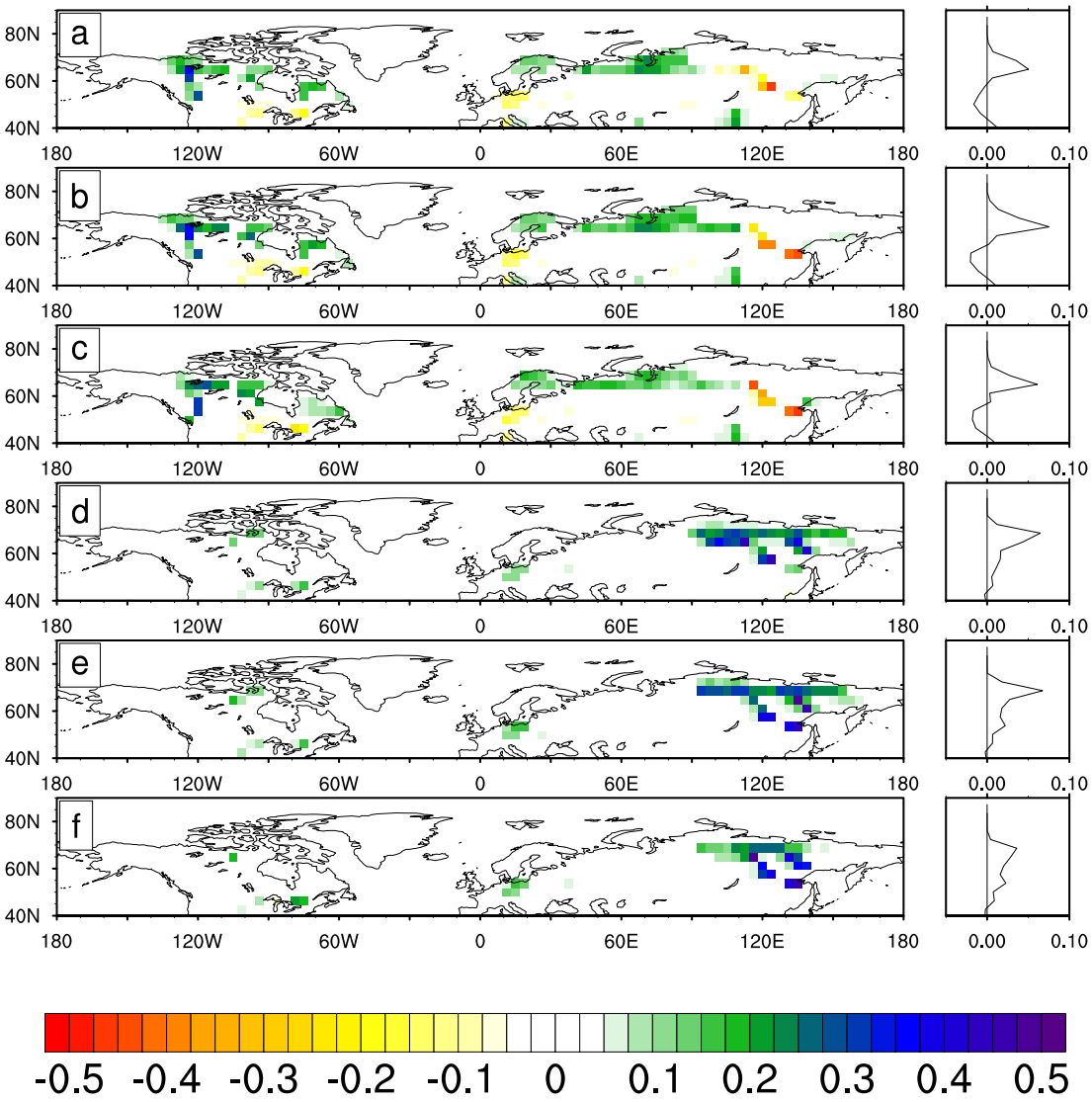

Figure 4.4: Change in forest fraction for evergreen forest (a – c) and deciduous forest (d – f) between mid-Holocene and pre-industrial for ΔAV (a, d), $\Delta AVsm$ (b, e), $\Delta AVsa$ (c, f). The right panel shows the zonal average of vegetation cover.

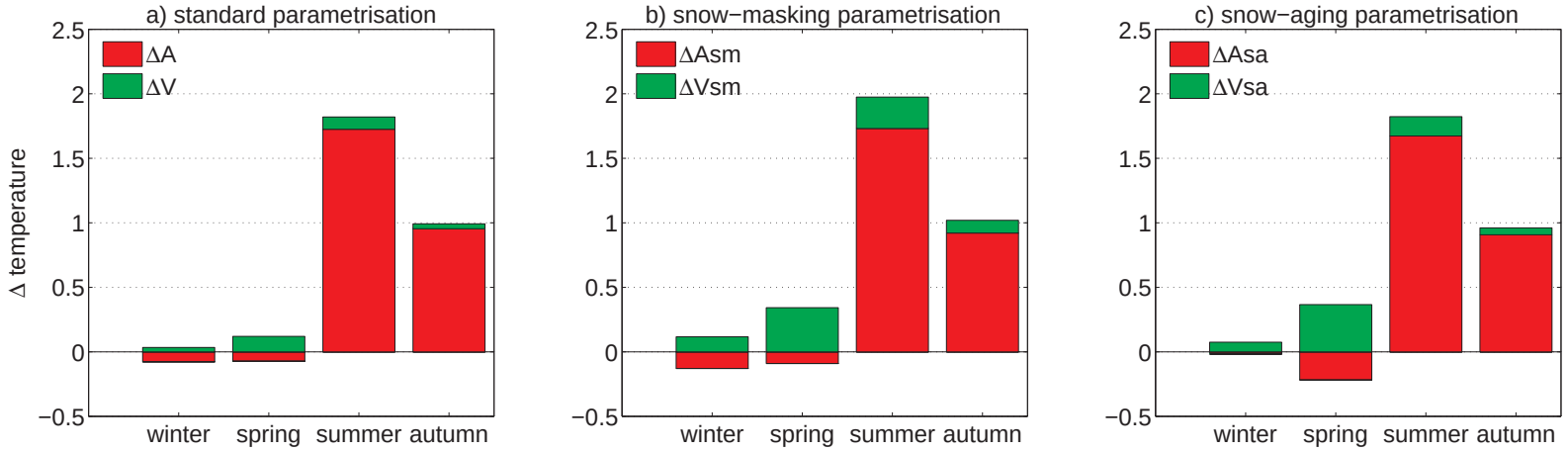

Figure 4.5: Seasonal air-temperature difference between mid-Holocene and pre-industrial climate averaged over land of the region $\geq 60^{\circ}$N for the atmospheric signal and the contribution of the vegetation for the model with standard parametrisation (a), the model with strong snow masking (b), the snow-aging model (c).

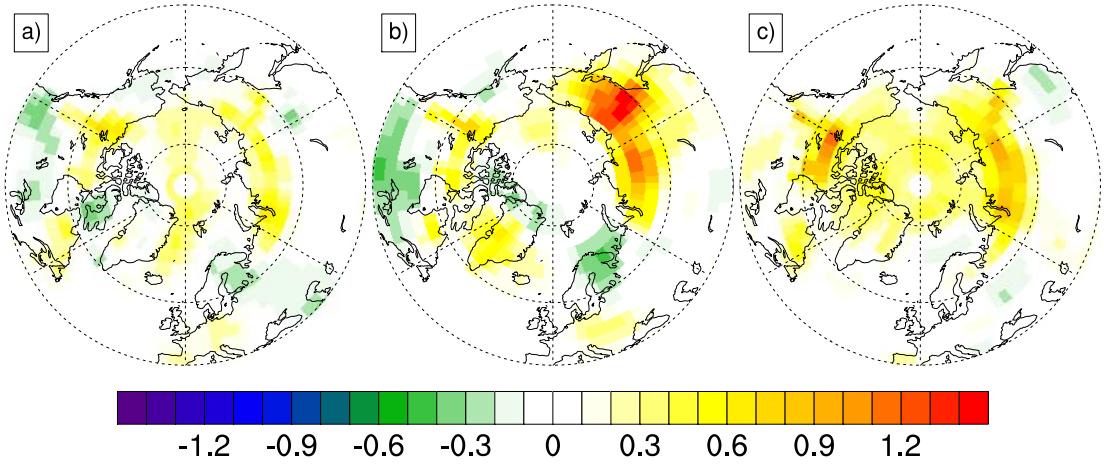

Figure 4.6: Mean spring air-temperature for $\Delta V[T]$ (a), $\Delta Vsm[T]$ (b), $\Delta Vsa[T]$ (c).

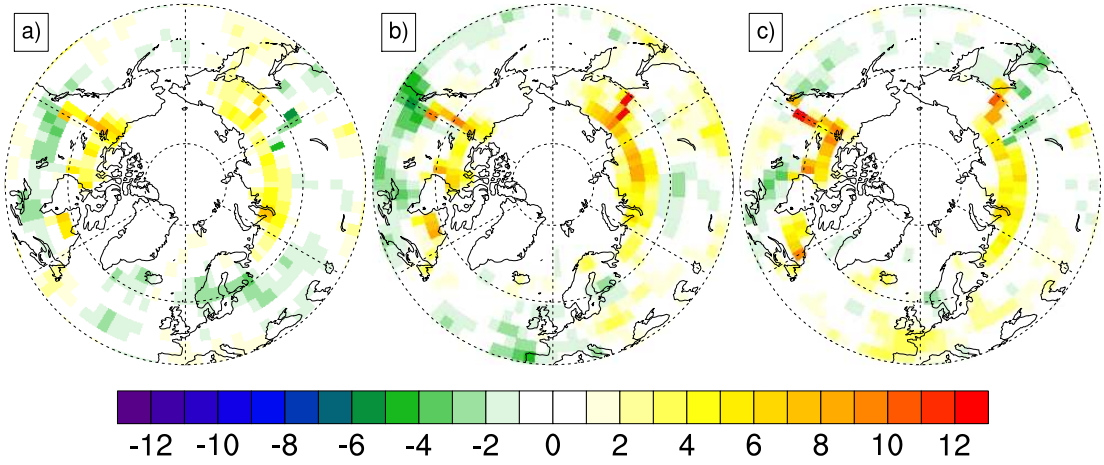

Figure 4.7: Mean spring net surface solar radiation in W/m^2 for $\Delta V[S]$ (a), $\Delta Vsm[S]$ (b), $\Delta Vsa[S]$ (c).

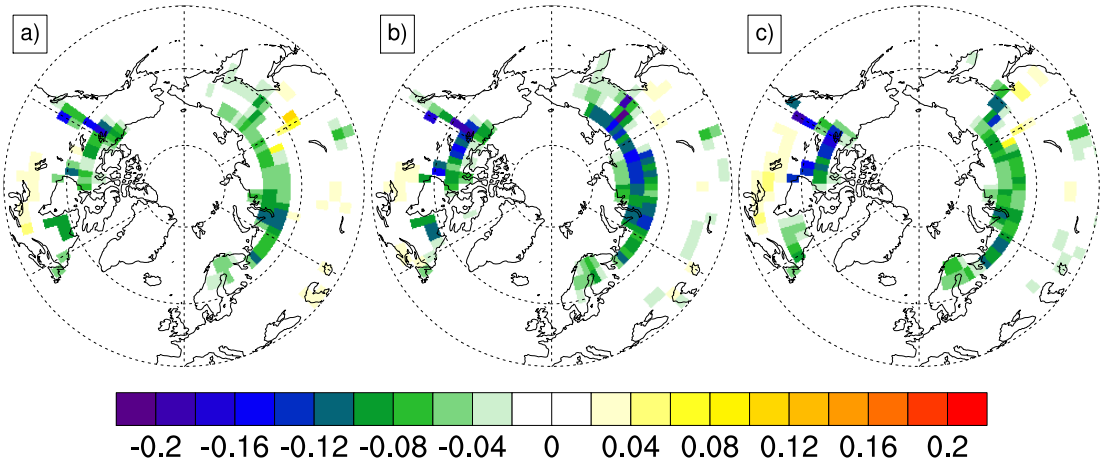

Figure 4.8: Mean spring surface albedo for $\Delta V[\alpha]$ (a), $\Delta Vsm[\alpha]$ (b), $\Delta Vsa[\alpha]$ (c).

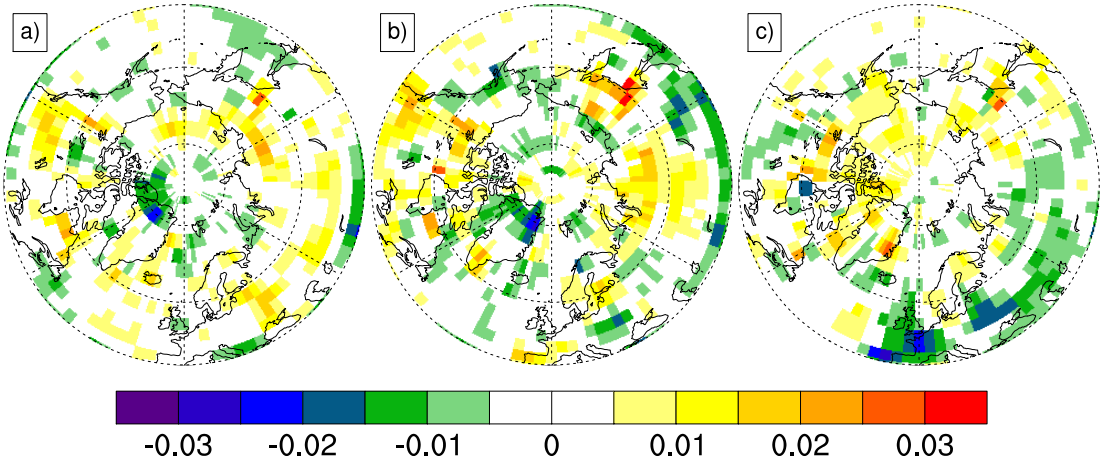

Figure 4.9: Mean spring total cloud cover as fraction for $\Delta V[Cl]$ (a), $\Delta Vsm[Cl$ (b), $\Delta Vsa[Cl$ (c).

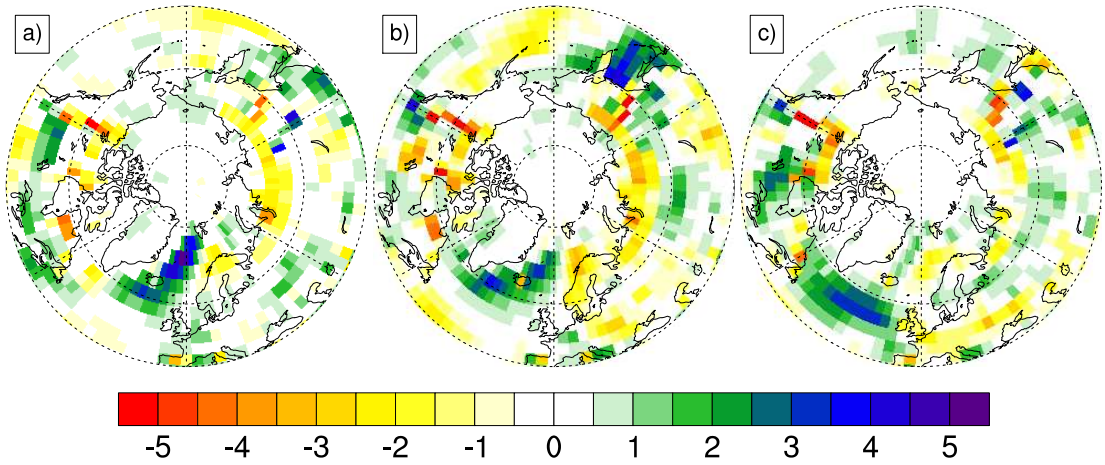

Figure 4.10: Mean spring sensible heat flux in W/m^2 for $\Delta V[SF]$ (a), $\Delta Vsm[SF]$ (b), $\Delta Vsa[SF]$ (c). Please note that upward fluxes are counted negatively. It follows that positive values indicate a reduction of flux in the mid-Holocene simulations.

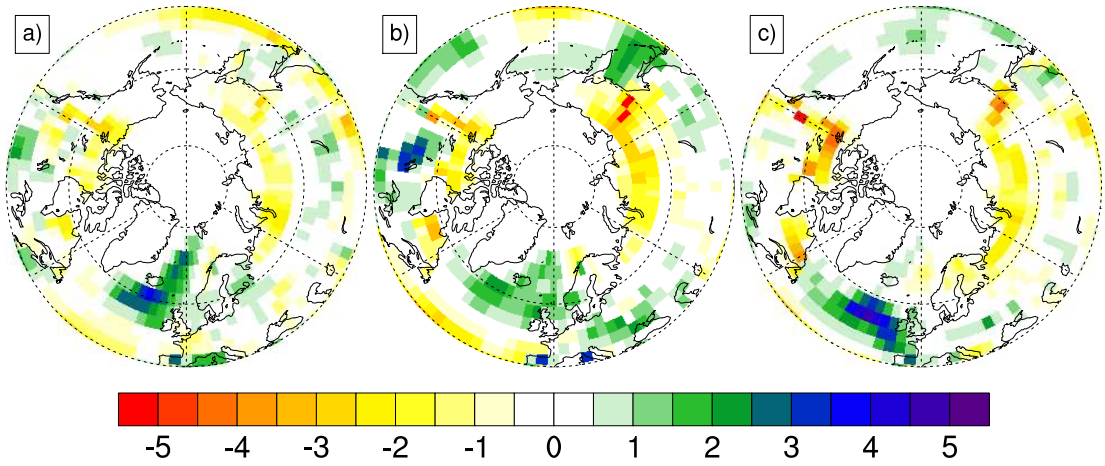

Figure 4.11: Mean spring latent heat flux in W/m^2 for $\Delta V[LF]$ (a), $\Delta Vsm[LF]$ (b), $\Delta Vsa[LF]$ (c). Please note that upward fluxes are counted negatively. It follows that positive values indicate a reduction of flux in the mid-Holocene simulations.

includes the largest strength of snow masking of deciduous forest (see Figure 4.1).
The change in surface albedo, however, cannot explain the regions with a decrease in net solar surface radiation (Figure 4.7). Thus, the atmospheric transmissivity must have changed. In general, clouds prevent solar radiation from entering the Earth's surface. Figure 4.9 depicts the total cloud cover anomaly in spring. The cloud cover is increased by up to 0.03 in the regions where forest has increased. The maximum cloud cover occurs over North-Eastern Siberia simulated with the model with strong snow masking. Nevertheless, cloud cover increases not only in regions with forest expansion but also south of these regions where no vegetation has changed. This feature is particularly prominent in the standard and snow-masking model (Figure 4.9 a,b).
The question why the cloud cover increases arises. In spring, trees start to sprout, leaves emerge and thus, transpiration increases (Schwartz and Karl 1990; Beringer et al. 2005; Chapin et al. 2000) as forest replaces mainly cold desert (Table 4.3). Figure 4.10 and Figure 4.11 show that both the sensible and the latent flux increases in the region of forest expansion. We cannot derive from the increase in latent heat flux if forest has a higher capability to transpire compared to other vegetation types. Nevertheless, the expansion of forest causes an increase in net surface solar radiation which favours stronger latent heat flux compared to the pre-industrial climate. Assuming that there is sufficient mixing within the atmospheric boundary layer to bring the moister air to its lifting condensation level, increased cloudiness results. The increased cloudiness reduces the solar downward radiation. This results in reduced net surface solar radiation at the surface of the Earth and thus less thermal energy is available for heating the atmosphere. This effect dampens the increase in net surface solar radiation by the reduced surface albedo in the boreal region. Thus, the spring warming is weakened. In regions without vegetation change, however, the increase in cloud fraction (Figure 4.9) results in a cooling because less energy is available for the atmospheric heating compared to present day.

4.4 Discussion of Chapter 4

During the mid-Holocene, the forest extended further northwards than in pre-industrial climate (e.g. MacDonald et al. (2000)), mainly due to the increased insolation during summer and early autumn. Several studies have associated this with a positive feedback (Foley et al. 1994; Texier et al. 1997; Claussen 2004; Wohlfahrt et al. 2004). Likely, this expansion led to a reduction in albedo due to the snow masking of forest, which favours the absorption of more solar radiation especially in spring. We test this statement by comparing the simulated net surface downward radiation signal $\Delta V[S]$ of the pure contribution of the atmosphere-vegetation feedback in spring with a simple estimate of the change in net surface solar radiation (S_{est}) due to the strength of snow masking and the change in forest. In particular, we multiply the solar downward radiation of $0kA$ by the strength of the snow masking for evergreen and deciduous forest, respectively, (see Figure 4.1, left column) and by the change in forest for evergreen and deciduous

forest, respectively, between the mid-Holocene and pre-industrial simulations (ΔAV) and average this product for the spring season:

$$S_{est} = \int_{t_1}^{t_2} S\downarrow (\delta\alpha_e \cdot \Delta f_e + \delta\alpha_d \cdot \Delta f_d)\ dt/(t_2 - t_1) \tag{4.4}$$

where $S\downarrow$ is the solar downward radiation in W/m^2 for $0k$, $\delta\alpha_e$ is the strength of snow masking of evergreen forest, $\delta\alpha_d$ is the strength of snow masking of deciduous forest, Δf_e the change in evergreen forest cover and Δf_d the change in deciduous forest cover between $6k$ and $0k$, and t_1 represents the date of the beginning of spring and t_2 the date of the end of spring. Figure 4.12 compares the estimated net surface solar radiation S_{est} with the simulated net surface solar radiation $\Delta V[S]$. The patterns of change in net surface solar radiation are very similar. However, S_{est} reveals a stronger increase in net surface solar radiation compared to the simulated net surface solar radiation by about a factor of two. In addition, S_{est} does not produce the reduction in net surface solar radiation of the region over North America between 40-60°N and North-East Europe. This indicates that the net surface solar radiation is weakened by a process which is not included in the simple estimate (equation 4.4). This missing process is the increase in transpiration by forest as discussed in Section 4.3.2. Therefore, we can support the statement that expansion of forest and its snow masking are the main land component drivers of the atmosphere-vegetation feedback (Otterman et al. 1984; Harvey 1988). However, the enhanced transpiration due to the expansion of forest area dampens the positive atmosphere-vegetation feedback (Claussen 2004; Pitman 2003).

The positive atmosphere-vegetation feedback causes a spring warming as shown by all three model configurations. However, the magnitude of the warming differs between the simulations with the different parametrisations. The snow-masking model reveals the largest spring temperature increase regionally (Figure 4.6). In North-Eastern Siberia, the temperature of the model with strong snow masking exceeds the temperature anomaly of the model with standard parametrisation by circa 1 °C. The snow-aging model increases the spring temperature response equally circumpolar by up to 0.5 °C compared to the model with standard parametrisation. However, the snow-aging model depicts a weaker regional temperature anomaly compared to the model with strong snow masking. The spring air-temperature averaged over the region north of 60°N reveals a slightly different picture. Both the snow-masking and the snow-aging model exhibit a similarly strong spring warming averaged over this region (ΔVsm = 0.34 °C, ΔVsa = 0.37 °C in spring). This is due to regions with larger and more pronounced cooling patterns in the snow-masking model compared to in the snow-aging model. However, both parametrisations enhance the spatial average temperature increase due to the atmosphere-vegetation feedback compared to the model with standard parametrisation (ΔV = 0.12 °C) by about a factor of three.

Strikingly, the simulations with the snow-aging model produce, with the smallest expansion of forest (9.25 x 10^5 km^2), the strongest increase in spatially averaged temperature (ΔVsa = 0.37). The strength of snow masking was enhanced by about 75%

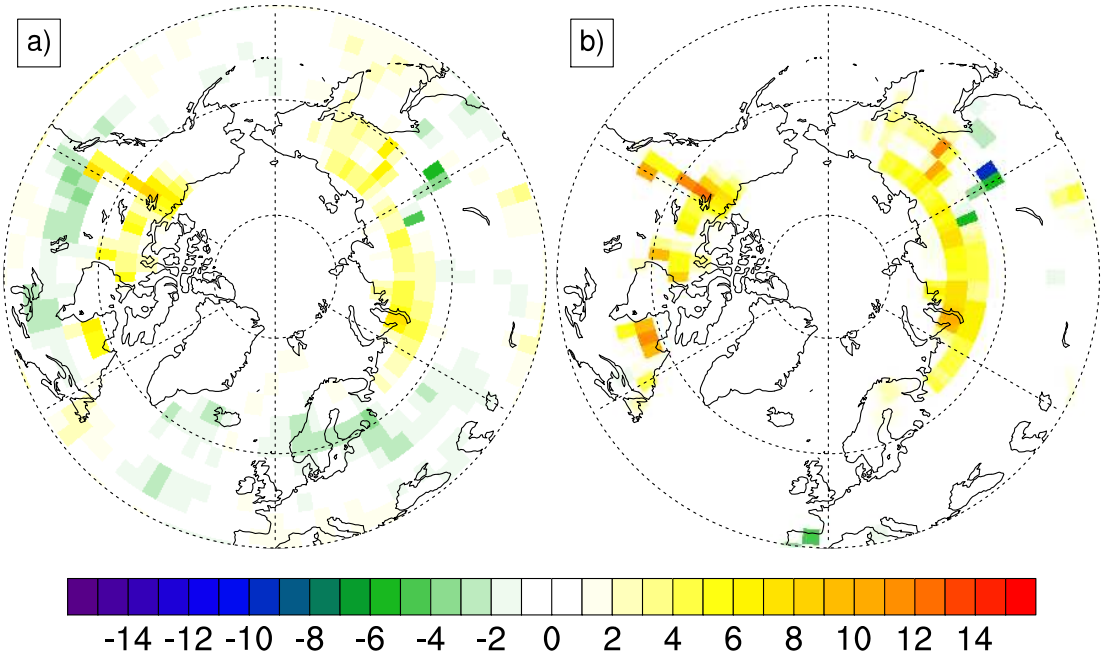

Figure 4.12: Comparison of spring net surface radiation for $\Delta V[S]$ (a) with the calculated net surface radiation S_{est} (b) derived from the solar downward radiation for 0k, the change in forest fraction from 0k to 6k and the strength of the snow masking.

for deciduous forest compared to the relative strength of snowmasking of 0.20 of the standard parametrisation. The strength of snow masking of evergreen forest was enhanced by about 20% relative to 0.50 of the standard parametrisation (see Figure 4.1). In the parametrisation with strong snow masking, we increased the strength of snow masking for evergreen forest only by 10% but more than doubled the strength of snow masking for deciduous forest relative to the standard parametrisation. With this snow-masking parametrisation, forest area increase is stronger by 3.47 x 10^5 km^2 but the temperature averaged over the region north of 60°N is 0.03 °C lower compared to the snow-aging model. This indicates that not only the amount of increased forest but also the parametrisation of the albedo of snow influence the strength of the atmosphere-vegetation feedback.

Despite the enhancement of the pure contribution of the atmosphere-vegetation feedback through the changes in the snow-albedo parametrisation, previous studies suggest a stronger contribution of the atmosphere-vegetation feedback to the mid-Holocene climate signal (Table 4.4). Simulations with the EMIC CLIMBER-2 by Ganopolski et al. (1998) exhibit a warming of up to 2.5 °C (60-70°N) in winter by the atmosphere-vegetation feedback due to a strong forest expansion in their mid-Holocene simulations. Ganopolski et al. (1998) obtained a factor of three more increase in forest than we simulated (Table 4.4). This strong warming of the atmosphere-vegetation feedback and the large expansion of forest is corroborated by Crucifix et al. (2002). Their study,

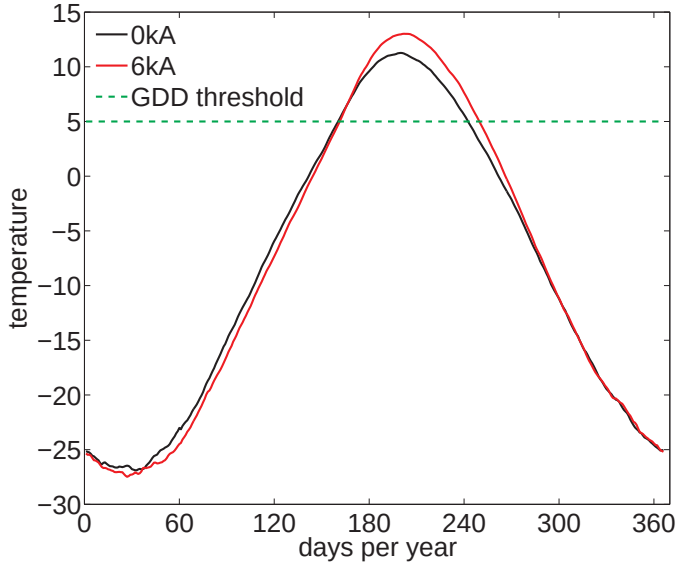

Figure 4.13: Daily mean temperature over land for $0kA$ and $6kA$ averaged over the region 60-70°N with the temperature threshold for growing degree days (GDD).

region	*spring temperature*	*change in forest in 10^5 km^2*	*model*	*citation*
≥ 60°N	0.12 °C	11.29	ECHAM5/JSBACH model with standard parametrisation	this study
≥ 60°N	0.34 °C	12.72	model with strong snow masking	this study
≥ 60°N	0.37 °C	9.25	snow-aging model	this study
≥ 60°N	*0.40 °C	[+58%]	FOAM-LPJ	Gallimore et al. (2005)
≥ 40°N	0.95 °C	6.50	IPSL-BIOME1	Wohlfahrt et al. (2004)
≥ 60°N	5.00 °C	46.00	MoBidiC	Crucifix et al. (2002)
≥ 60°N	[not given]	30.00	CLIMBER-2	Ganopolski et al. (1998)
≥ 60°N	*3.30 °C	[prescribed]	GENESIS	Foley et al. (1994)

Table 4.4: Summary of spring air-temperature differences between 6k and 0k of the atmosphere-vegetation feedback simulated by our study and simulated by previous studies. Values marked with (*) indicate that this value includes the climate response of an interactive ocean.

performed with the EMIC MoBidiC, produces a very strong warming of 5 °C north of 60°N in spring and an expansion of forest by about a factor of four more than we simulated (Table 4.4). However, the authors refer to this strong warming as unrealistic, as their model reveals a tendency to overestimate the impact of insolation forcing on vegetation. The discrepancy between our comparable weak increase in forest to the large expansion of forest in EMICs may be the result of the higher resolution of our model compared to the coarse resolution of the utilised EMICs. The resolution of our model is approximately 3.75 ° at the equator. Commonly, EMICs distinguish only between two vegetation types (trees and grass) per grid box with a resolution of 10 ° in latitude and 51 ° in longitude (Ganopolski et al. 1998). A grid box of this size covers a larger area with either grass or forest than in JSBACH. When the climate changes, for instance due to mid-Holocene insolation forcing, the vegetation cover of each grid box adapts to it and, thus, causes a stronger increase in e.g. forest than simulated with our higher-resolved model.

Simulations with GCMs reveal a weaker contribution of the atmosphere-vegetation feedback than simulated with EMICs (see Table 4.4). A study (Gallimore et al. 2005) with the GCM FOAM-LPJ produces a atmosphere-vegetation feedback of 0.40 °C. Gallimore et al. (2005) explain this weak warming with a large mid-latitude expansion of grass cover outweighing the expansion in boreal forest cover in their model and therefore weakening the atmosphere-vegetation feedback. This is not the case in our model as we do not simulate an expansion of grass in the mid-latitudes. Wohlfahrt et al. (2004) coupled the vegetation model BIOME1 asynchronously with the GCM IPSL. Their simulations show a spring warming that reaches 0.95 °C averaged over the region north 40°N with an expansion of forest only half of our simulated increase in forest. In comparison to the study by Wohlfahrt et al. (2004), we use a GCM including a fully coupled vegetation module. The vegetation module follows a tiling approach (Brovkin et al. 2009), so that on each of the model's grid boxes, a mosaic of different vegetation types can exist. The vegetation composition is temporally variable and derived from succession processes such as establishment and mortality. Wohlfahrt et al. (2004), however, used a vegetation module asynchronously coupled with a GCM. In their approach, each grid box contained only one type of vegetation. With a climate change, a whole grid box changes, for example to forest, whereas with the tiling approach only a fraction of the grid box is turned into forest. The temperature response to these large-scale changes is stronger compared to the fractional change in vegetation cover in our model.

Another factor controlling the forest cover in climate models is the warmth of the growing season. Commonly, the forest cover is determined as a function of growing degree days (GDD) which is defined as the sum of daily mean air-temperature above the threshold of 5 °C. In our model, the growing season of the mid-Holocene is characterised by higher temperatures and a prolongation of six days compared to the pre-industrial climate (Figure 4.13). However, these limits show also that the increase of forest is limited by these values and spatially by the coast (Figure 4.4).

The question arises how well our model simulates the expansion of forest in comparison to reconstructions. Reconstructions of the mid-Holocene treeline suggest an asymmetric response of the vegetation to the change in insolation (MacDonald et al. 2000; Bigelow et al. 2003). The reconstructions show northward shifts of forest by up to 200 km in central Siberia, and 50-100 km in Western Europe and in North-West Canada. For Eastern Canada, reconstruction suggest that the tree line was further south than present. The simulated northward extension of forest areas for the mid-Holocene is in general agreement with the reconstructions (see Figure 4.4). The increase in deciduous forest in Eastern Siberia is also supported by reconstructions (Texier et al. 1997). Wohlfahrt et al. (2008) presented an evaluation of GCM simulations of the mid-Holocene with palaeovegetation data. In their study, the different GCMs simulate an increase in forest between 6 - 16 x 10^5 km^2 north of 60°N. Our results with an increase in forest between 9 - 13 x 10^5 km^2 (see Table 4.4) are in the range of the results by Wohlfahrt et al. (2008).

To summarise, with our model setup ECHAM5/JSBACH we cannot corroborate the suggestion of a strong atmosphere-vegetation feedback, neither with the model with standard parametrisation nor with the modified parametrisations with the changes in the scheme of the albedo of snow. Dallmeyer et al. (2010) used the same model and setup and found only a weak contribution of the vegetation to the mid-Holocene climate signal for monsoonal Asia as well. The weak contribution of the atmosphere-vegetation feedback in our model is mainly a result of the comparatively weak forest expansion in contrast to studies with EMICs with a coarser resolution. Presumably, climate models with a higher resolved and dynamic representation of vegetation cover simulate a weaker atmosphere-vegetation feedback than simulated with EMICs and GCMs with an asynchronously coupled and discrete vegetation model. Therewith, our results rather support the conclusion of the Palaeoclimate Modelling Intercomparison Project 2 (PMIP2) (Braconnot et al. 2007b), that the magnitude of the atmosphere-vegetation feedback is smaller than previously discussed.

Chapter 5

Conclusions and outlook

5.1 Conclusions

To conclude this thesis, we attempt to answer the questions raised in the introduction (Chapter 1).

(1) Using a comprehensive GCM and applying the factor-separation technique, how do we relate the mid-Holocene climate signal to the components of the climate system?

The full mid-Holocene climate signal of the model ECHAM5/JSBACH-MPIOM shows a modification of the seasonal cycle at the high northern latitudes compared to pre-industrial climate. This is characterised by warmer summer, autumn and winter, and a cooler climate in spring.
The direct response of the atmosphere to the change in insolation produces a summer warming which slightly decreases in autumn. The winter and spring seasons, however, show a cooling by the direct atmosphere signal.
The contribution of the atmosphere-vegetation feedback to the mid-Holocene temperature signal is rather marginal. In spring and summer it leads to a slight warming counteracting to the cooling caused by the direct atmospheric signal. The atmosphere-ocean feedback amplifies the atmospheric signal in spring and autumn and counteracts it slightly in summer and more strongly in winter. The synergy between the atmosphere-ocean and atmosphere-vegetation feedback results in a slight warming for all seasons.
In comparison to previous studies, we simulate a strong influence by the ocean but a weak influence by both the vegetation and the associated synergy on the mid-Holocene climate signal. The strong influence in autumn is caused by the orbitally-induced increase in summer and autumn insolation. Due to this increase more sea ice melts in summer and autumn and the ocean warms up more strongly than in the pre-industrial climate. During late autumn and winter, the ocean releases this heat to the atmosphere, resulting in higher air-temperatures compared to pre-industrial climate. This introduces a lag between the season cycle of insolation and oceanic response by approximately one season.

(2) Does the definition of the seasons effect the assignment of the mid-Holocene climate signal to the components of the climate system?

No, this is not the case for the contribution of the atmosphere-vegetation and atmosphere-ocean feedback and their synergy. However, this is the case for the seasonal direct atmospheric signal with the largest deviation in autumn. Previous studies suggested a cooling of the direct atmospheric signal in this season, but in our study, consistently following the insolation signal, we simulate a warming. Studies defining the seasons by the date of the vernal equinox fixed on 21 March, underestimated changes in the Northern Hemisphere in autumn and winter (Braconnot et al. 2007a). This amounts to 0.9 °C in autumn and 0.2 °C in winter according to our data processed with the date of the vernal equinox fixed on 21 March. This result supports the claim by Joussaume and Braconnot (1997) and Timm et al. (2008) that in palaeo-climate modelling, the precise definition of the season is essential.

(3) Does statistical uncertainty introduced by climate variability lead to divergent model results?

We have performed several sets of simulations to quantify how the statistical uncertainty affects the estimated atmosphere-vegetation and atmosphere-ocean feedback and their synergy to mid-Holocene insolation. Although the analysis period is 120 years long, it leads to statistical uncertainty which has different effects on the magnitude of the feedbacks. The atmosphere response and the atmosphere-vegetation feedback are statistically robust features. By contrast, the factors derived from simulations with an interactive ocean are sensitive to long-term anomalies in sea-ice cover. As a result, GCM simulations with an interactive ocean should include a long spin-up time as well as a long analysis period to reduce the statistical uncertainty. This is also important with regard to model intercomparison studies. Nevertheless, this study confirms that, according to our model, the most important modification of the orbital forcing can be firmly related to the atmosphere-ocean interactions. The divergent results of mid-Holocene studies can therefore only partly be related to internal variability.

(4) To what extent does the strength of the atmosphere-vegetation feedback depend on the snow-albedo parametrisation?

The atmosphere-vegetation feedback evokes two opposing effects in spring. Firstly, the expansion of forest leads to a reduction in surface albedo which favours a warming. Secondly, the expansion of forest enhances transpiration and thus an increase in cloud fraction which favours a cooling. Nevertheless, in spring the atmosphere-vegetation feedback produces a warming which is stronger than the cooling effect. Possibly, similar processes consitute the atmosphere-vegetation feedback in other climate models but

presumably to divering extent.
The magnitude of the warming of the atmosphere-vegetation feedback depends to a certain extent on the parametrisation of the albedo of snow. The increase in the strength of snow masking by deciduous trees results in a strong regional response in temperature. Simulations with the snow albedo depending on the age of snow show also a strong regional response in temperature. However, on the large-scale the temperature signal of the atmosphere-vegetation feedback is weak compared to previous modelling studies.
As discussed by Claussen (2009), it is not possible to draw a clear conclusion regarding the magnitude of the atmosphere-vegetation feedback. We argue that the strength of the atmosphere-vegetation feedback was overestimated by climate models with a coarse resolution and/or asynchronously coupled with a vegetation model. With the further development of models (e.g. gradually resolved vegetation cover by a tiling approach (Brovkin et al. 2009)), the biogeophysical atmosphere-vegetation feedback has become less strong.
To support this conclusion that the atmosphere-vegetation feedback is weaker than previously suggested, a similar study with another GCM including a dynamic vegetation model would be helpful. In addition, the coupling strength between the land-surface and the atmosphere model could be quantified. Koster et al. (2006) and Guo et al. (2006) showed with a model intercomparison study that the land-atmosphere coupling strength is a critical element of climate modelling. Their results reveal that the coupling strength varied widely between the 12 participating atmosphere-only GCMs. Hence, the strength of the atmosphere-vegetation feedback may depend not only on the parametrisation of the albedo of snow and on the horizontal resolution but also on the strength of land-atmosphere coupling in a climate model.

5.2 Outlook

To evaluate the strength of the atmosphere-vegetation feedback among different models, simulations with various atmosphere-ocean-vegetation GCMs following the same experiment setup as we did would help. Such intermodel comparison is one way to analyse the extent to which the experimental results are model-dependent. This could be done in a framework like for instance for human-induced land-cover change (Pitman et al. 2009). This model intercomparison showed that model results can be strongly model-dependent. Pitman et al. (2009) could not derive concordant results across seven GCMs because of the lack of consistency among the models.
It has been suggested that global warming might enhance future warming in boreal forest via the positive atmosphere-vegetation feedback (O'ishi and Abe-Ouchi 2009) as elaborated in this study for the mid-Holocene. Thus, the atmosphere-vegetation feedbacks may be important in determining the future climate. For example, Levis et al. (2000) showed that vegetation feedbacks under a double CO_2 climate could produce an additional 3 °C warming during spring in the region north of 60°N. This is supported

by O'ishi et al. (2009) showing that the inclusion of dynamic vegetation leads to an amplification of global warming climate sensitivity (quadrupling of CO_2) by 13%.
One limitation of this study is that we examined the vegetation feedback by fixing only the vegetation cover (e.g. leaf phenology is not included in the atmosphere-vegetation feedback). The continued examination of the atmosphere-vegetation feedback will have to consider the role of changes in seasonal leaf phenology as well as soil properties. On the other hand, not only the biogeophysical atmosphere-vegetation feedback but also the biogeochemical atmosphere-vegetation feedback needs to be taken into account (Claussen et al. 2001). The uptake and release of CO_2 by vegetation is of particular interest for future climate simulations (Schurgers et al. 2008). The question which role the biogeophysical feedback and the biogeochemical feedback play has not been solved (Claussen 2009). Both feedbacks can be positive or negative and therefore partly compensate each other. Thus, to examine the entire atmosphere-vegetation interaction both feedbacks need to be considered in the future analysis.
A comparison of model results against modern observations will help to improve the knowledge about the atmosphere-vegetation feedback. For instance, Notaro and Liu (2008) demonstrated this with an analysis of the atmosphere-vegetation feedback over Asiatic Russia through a combined statistical and dynamical approach. In addition, parametrisations that describe the Earth's continental surfaces more accurately according to observations may improve the simulation of feedbacks and climate sensitivity (Levis et al. 2007; Qu and Hall 2007). To conclude, a model inter-comparison study constrained by palaeo-reconstructions, and in combination with modern observations will improve our understanding of past and present climate change.

.

Appendix A

Snow-aging albedo scheme

The key parameter in the BATS formulation for snow albedo (Dickinson et al. 1986) is the snow aging factor f_{age} which is defined as

$$f_{age} = \frac{\tau_s}{1 + \tau_s} \tag{A.1}$$

where τ_s is a nondimensional age of snow, defined as

$$\tau_s{}^{N+1} = (\tau_s{}^{N} + \Delta\tau_s)\left[1 - \frac{\max(0, \Delta S_n)}{\Delta P_s}\right] \tag{A.2}$$

where N denotes the current time step, ΔS_n is the change of snow water equivalent (in mm) in one time step Δt, and $\Delta P_s = 10\ kg/m^2$ is the amount of fresh snow which is required to refresh snow albedo. This means that a snowfall of 10 mm water equivalent, or more, is assumed to restore the surface age which increases the snow albedo to its maximum value.
$\Delta\tau_s$ is parameterized as

$$\Delta\tau_s = (r_1 + r_2 + r_3)\frac{\Delta t}{\tau_0} \tag{A.3}$$

where $\tau_0 = 10^6 s \times r_1$ represents the effect of grain growth due to vapour diffusion and is expressed as

$$r_1 = \exp\left[5000(\frac{1}{273.16} - \frac{1}{T_s})\right] \tag{A.4}$$

where T_s is the surface temperature; r_2 represents the additional effect of grain growth near or at the freezing of meltwater,

$$r_2 = (r_1)^{10} \leq 1 \tag{A.5}$$

and r_3 represents the effect of dirt and soot,

$$r_3 = \begin{cases} 0.01 & \text{over Antarctica} \\ 0.3 & \text{elsewhere.} \end{cases} \tag{A.6}$$

The parametrisation of snow albedo is based on (Wiscombe and Warren 1980):

$$\alpha_{VIS} = \alpha_{VIS,D} + 0.4 f(\psi)[1 - \alpha_{VIS,D}] \tag{A.7}$$

$$\alpha_{NIR} = \alpha_{NIR,D} + 0.4 f(\psi)[1 - \alpha_{NIR,D}] \tag{A.8}$$

where ψ is the solar zenith angle, α_{VIS} the albedo for $\lambda < 0.7\ \mu m$ and NIR the albedo for $\lambda \geq 0.7\ \mu m$. The subscript D denotes diffuse albedo as given by

$$\alpha_{VIS,D} = [1 - C_S f_{age}]\alpha_{VIS,0} \tag{A.9}$$

$$\alpha_{NIR,D} = [1 - C_N f_{age}]\alpha_{NIR,0} \tag{A.10}$$

where $C_S = 0.2$ and $C_N = 0.5$. In order to avoid changes in the long-term mean climate, we increased the snow albedo from $C_S = 0.2$ (Dickinson et al. 1986) to $C_S = 0.3$. The albedos for visible and near-infrared solar radiation incident on new snow with a solar zenith angle less than 60° are $\alpha_{VIS,0} = 0.95$ and $\alpha_{NIR,0} = 0.65$. The function f_{age} is defined in Equation A.1 is a factor between 0 and 1, giving the increase of snow visible albedo when the solar zenith angle exceeds 60°:

$$f(\psi) = \frac{1}{b}\left[\frac{1+b}{1+2b\cos(\psi)} - 1\right] \tag{A.11}$$

where $b = 2$. If $\cos(\psi) > 0.5$ then $f(\psi) = 0$.
The validation of the BATS snow scheme and implementation details are described in Roesch (1999).

Bibliography

Barlage, M., Zeng, X. B., Wei, H. L., and Mitchell, K. E.: A global 0.05 degrees maximum albedo dataset of snow-covered land based on MODIS observations, Geophysical Research Letters, 32, L17 405, 2005.

Bates, J. R.: Some considerations of the concept of climate feedback, Quarterly Journal Of The Royal Meteorological Society, 133, 545–560, 2007.

Bengtsson, L., Semenov, V. A., and Johannessen, O. M.: The early twentieth-century warming in the Arctic - A possible mechanism, Journal Of Climate, 17, 4045–4057, 2004.

Berger, A.: Long-Term Variations Of Daily Insolation And Quaternary Climatic Changes, J. Atmos. Sci., 35, 2362–2367, 1978.

Berger, A.: The role of CO2, sea level, and vegetation during the Milankovitch-forced glacial-interglacial cycles, In: Bengtsson and L., Hammer, C. (editors), Geosphere-Biosphere Interactions and Climate, Cambridge Univ. Press, 2001.

Berger, A.: Factor separation method and palaeoclimates, In: P. Alpert and T. Sholokhman, (editors), Factor Separation in the Atmosphere-Applications and Future Prospects, Cambridge Univ. Press, in press.

Beringer, J., Chapin, F. S., Thompson, C. C., and McGuire, A. D.: Surface energy exchanges along a tundra-forest transition and feedbacks to climate, Agricultural And Forest Meteorology, 131, 143–161, 2005.

Betts, A. K. and Ball, J. H.: Albedo over the boreal forest, J. Geophys. Res., 102, 28 901–28 909, 1997.

Bigelow, N. H., Brubaker, L. B., Edwards, M. E., Harrison, S. P., Prentice, I. C., Anderson, P. M., Andreev, A. A., Bartlein, P. J., Christensen, T. R., Cramer, W., Kaplan, J. O., Lozhkin, A. V., Matveyeva, N. V., Murray, D. F., McGuire, A. D., Razzhivin, V. Y., Ritchie, J. C., Smith, B., Walker, D. A., Gajewski, K., Wolf, V., Holmqvist, B. H., Igarashi, Y., Kremenetskii, K., Paus, A., Pisaric, M. F. J., and Volkova, V. S.: Climate change and Arctic ecosystems: 1. Vegetation changes north of 55 degrees N between the last glacial maximum, mid-Holocene, and present, J. Geophys. Res., 108, 8170, 2003.

Bony, S., Colman, R., Kattsov, V. M., Allan, R. P., Bretherton, C. S., Dufresne, J. L., Hall, A., Hallegatte, S., Holland, M. M., Ingram, W., Randall, D. A., Soden, B. J., Tselioudis, G., and Webb, M. J.: How well do we understand and evaluate climate change feedback processes?, J. Climate, 19, 3445–3482, 2006.

Braconnot, P., Otto-Bliesner, B., Harrison, S., Joussaume, S., Peterchmitt, J. Y., Abe-Ouchi, A., Crucifix, M., Driesschaert, E., Fichefet, T., Hewitt, C. D., Kageyama, M., Kitoh, A., Laine, A., Loutre, M. F., Marti, O., Merkel, U., Ramstein, G., Valdes, P., Weber, S. L., Yu, Y., and Zhao, Y.: Results of PMIP2 coupled simulations of the mid-Holocene and Last Glacial Maximum - Part 1: experiments and large-scale features, Clim. Past, 3, 261–277, 2007a.

Braconnot, P., Otto-Bliesner, B., Harrison, S., Joussaume, S., Peterchmitt, J. Y., Abe-Ouchi, A., Crucifix, M., Driesschaert, E., Fichefet, T., Hewitt, C. D., Kageyama, M., Kitoh, A., Loutre, M. F., Marti, O., Merkel, U., Ramstein, G., Valdes, P., Weber, L., Yu, Y., and Zhao, Y.: Results of PMIP2 coupled simulations of the mid-Holocene and Last Glacial Maximum - Part 2: feedbacks with emphasis on the location of the ITCZ and mid- and high latitudes heat budget, Clim. Past, 3, 279–296, 2007b.

Brovkin, V., Levis, S., Loutre, M. F., Crucifix, M., Claussen, M., Ganopolski, A., Kubatzki, C., and Petoukhov, V.: Stability analysis of the climate-vegetation system in the northern high latitudes, Climatic Change, 57, 119–138, 2003.

Brovkin, V., Raddatz, T., Reick, C. H., Claussen, M., and Gayler, V.: Global biogeophysical interactions between forest and climate, Geophysical Research Letters, 36, L07 405, 2009.

Chapin, F. S., McGuire, A. D., Randerson, J., Pielke, R., Baldocchi, D., Hobbie, S. E., Roulet, N., Eugster, W., Kasischke, E., Rastetter, E. B., Zimov, S. A., and Running, S. W.: Arctic and boreal ecosystems of western North America as components of the climate system, Global Change Biology, 6, 211–223, 2000.

Cheddadi, R., Yu, G., Guiot, J., Harrison, S. P., and Prentice, I. C.: The climate of Europe 6000 years ago, Climate Dyn., 13, 1–9, 1996.

Claussen, M.: The Global Climate - Chapter A.4, In: Kabat, P., Claussen, M., Dirmeyer, P.A., Gash, J.H.C., Guenni, L., Meybeck, M., Pielke, R.A., Vörösmarty, C.J., Lütkemeier, S. (editors), Vegetation, Water, Humans and the Climate: A New Perspective on an Interactive System, Springer-Verlag Heidelberg, 2004.

Claussen, M.: Late Quaternary vegetation-climate feedbacks, Climate Of The Past, 5, 203–216, 2009.

Claussen, M., Kubatzki, C., Brovkin, V., Ganopolski, A., Hoelzmann, P., and Pachur, H. J.: Simulation of an abrupt change in Saharan vegetation in the mid-Holocene, Geophysical Research Letters, 26, 2037–2040, 1999.

Claussen, M., Brovkin, V., and Ganopolski, A.: Biogeophysical versus biogeochemical feedbacks of large-scale land cover change, Geophys. Res. Lett., 28, 1011–1014, 2001.

Claussen, M., Fohlmeister, J., Ganopolski, A., and Brovkin, V.: Vegetation dynamics amplifies precessional forcing, Geophys. Res. Lett., 33, L09 709, 2006.

Crucifix, M., Loutre, M. F., Tulkens, P., Fichefet, T., and Berger, A.: Climate evolution during the Holocene: a study with an Earth system model of intermediate complexity, Climate Dyn., 19, 43–60, 2002.

Dallmeyer, A., Claussen, M., and Otto, J.: Contribution of oceanic and vegetation feedbacks to Holocene climate change in monsoonal Asia, Clim. Past, 6, 195–218, 2010.

Davis, B. A. S., Brewer, S., Stevenson, A. C., and Guiot, J.: The temperature of Europe during the Holocene reconstructed from pollen data, Quaternary Sci. Rev, 22, 1701–1716, 2003.

Delworth, T. L., Stouffer, R. J., Dixon, K. W., Spelman, M. J., Knutson, T. R., Broccoli, A. J., Kushner, P. J., and Wetherald, R. T.: Review of simulations of climate variability and change with the GFDL R30 coupled climate model, Climate Dynamics, 19, 555–574, 2002.

deNoblet, N. I., Prentice, I. C., Joussaume, S., Texier, D., Botta, A., and Haxeltine, A.: Possible role of atmosphere-biosphere interactions in triggering the last glaciation, Geophysical Research Letters, 23, 3191–3194, 1996.

Dickinson, R., Henderson-Sellers, A., Kennedy, P., and Wilson, M.: Biosphere-Atmosphere Transfer Scheme (BATS) for the NCAR community Climate Model., Ncar/tn-275+str., National Center for Atmospheric Research, Boulder, Colorado., 1986.

Diffenbaugh, N. S. and Sloan, L. C.: Global climate sensitivity to land surface change: The Mid Holocene revisited, Geophys. Res. Lett., 29, 1476, 2002.

Divine, D. and Dick, C.: Historical variability of sea ice edge position in the Nordic Seas, Journal of Geophysical Research-Part C-Oceans, 111, 14 pp., 2006.

Essery, R., Rutter, N., Pomeroy, J., Baxter, R., Stahli, M., Gustafsson, D., Barr, A., Bartlett, P., and Elder, K.: An Evaluation of Forest Snow Process Simulations, Bulletin Of The American Meteorological Society, 90, 2009.

Foley, J. A., Kutzbach, J. E., Coe, M. T., and Levis, S.: Feedbacks Between Climate And Boreal Forests During The Holocene Epoch, Nature, 371, 52–54, 1994.

Gallimore, R., Jacob, R., and Kutzbach, J.: Coupled atmosphere-ocean-vegetation simulations for modern and mid-Holocene climates: role of extratropical vegetation cover feedbacks, Climate Dyn., 25, 755–776, 2005.

Ganachaud, A. and Wunsch, C.: Improved estimates of global ocean circulation, heat transport and mixing from hydrographic data, Nature, 408, 453–457, 2000.

Ganopolski, A., Kubatzki, C., Claussen, M., Brovkin, V., and Petoukhov, V.: The influence of vegetation-atmosphere-ocean interaction on climate during the mid-Holocene, Science, 280, 1916–1919, 1998.

Guo, Z. C., Dirmeyer, P. A., Koster, R. D., Bonan, G., Chan, E., Cox, P., Gordon, C. T., Kanae, S., Kowalczyk, E., Lawrence, D., Liu, P., Lu, C. H., Malyshev, S., McAvaney, B., McGregor, J. L., Mitchell, K., Mocko, D., Oki, T., Oleson, K. W., Pitman, A., Sud, Y. C., Taylor, C. M., Verseghy, D., Vasic, R., Xue, Y. K., and Yamada, T.: GLACE: The Global Land-Atmosphere Coupling Experiment. Part II: Analysis, Journal Of Hydrometeorology, 7, 611–625, 2006.

Harvey, L. D. D.: On The Role Of High-Latitude Ice, Snow, And Vegetation Feedbacks In The Climatic Response To External Forcing Changes, Climatic Change, 13, 191–224, 1988.

Hewitt, C. D. and Mitchell, J. F. B.: A fully coupled GCM simulation of the climate of the mid-Holocene, Geophys. Res. Lett., 25, 361–364, 1998.

Jin, Y. F., Schaaf, C. B., Gao, F., Li, X. W., Strahler, A. H., and Zeng, X. B.: How does snow impact the albedo of vegetated land surfaces as analyzed with MODIS data?, Geophysical Research Letters, 29, 1374, 2002.

Joussaume, S. and Braconnot, P.: Sensitivity of paleoclimate simulation results to season definitions, J. Geophys. Res., 102, 1943–1956, 1997.

Jungclaus, J. H., Keenlyside, N., Botzet, M., Haak, H., Luo, J. J., Latif, M., Marotzke, J., Mikolajewicz, U., and Roeckner, E.: Ocean circulation and tropical variability in the coupled model ECHAM5/MPI-OM, J. Climate, 19, 3952–3972, 2006.

Kaplan, J. O., Bigelow, N. H., Prentice, I. C., Harrison, S. P., Bartlein, P. J., Christensen, T. R., Cramer, W., Matveyeva, N. V., McGuire, A. D., Murray, D. F., Razzhivin, V. Y., Smith, B., Walker, D. A., Anderson, P. M., Andreev, A. A., Brubaker, L. B., Edwards, M. E., and Lozhkin, A. V.: Climate change and Arctic ecosystems. 2. Modeling, paleodata-model comparisons, and future projections, Journal of Geophysical Research, 108, ALT12–1–17, 2003.

Kerwin, M. W., Overpeck, J. T., Webb, R. S., DeVernal, A., Rind, D. H., and Healy, R. J.: The role of oceanic forcing in mid-Holocene Northern Hemisphere climatic change, Paleoceanography, 14, 200–210, 1999.

Koenigk, T., Mikolajewicz, U., Jungclaus, J. H., and Kroll, A.: Sea ice in the Barents Sea: seasonal to interannual variability and climate feedbacks in a global coupled model, Climate Dynamics, 32, 1119–1138, 2009.

Koster, R. D., Guo, Z. C., Dirmeyer, P. A., Bonan, G., Chan, E., Cox, P., Davies, H., Gordon, C. T., Kanae, S., Kowalczyk, E., Lawrence, D., Liu, P., Lu, C. H., Malyshev, S., McAvaney, B., Mitchell, K., Mocko, D., Oki, T., Oleson, K. W., Pitman, A., Sud, Y. C., Taylor, C. M., Verseghy, D., Vasic, R., Xue, Y. K., and Yamada, T.: GLACE: The Global Land-Atmosphere Coupling Experiment. Part I: Overview, Journal Of Hydrometeorology, 7, 590–610, 2006.

Levis, S., Foley, J. A., and Pollard, D.: Large-scale vegetation feedbacks on a doubled CO2 climate, Journal Of Climate, 13, 1313–1325, 2000.

Levis, S., Bonan, G. B., and Lawrence, P. J.: Present-day springtime high-latitude surface albedo as a predictor of simulated climate sensitivity, Geophysical Research Letters, 34, L17 703, 2007.

MacDonald, G. M., Velichko, A. A., Kremenetski, C. V., Borisova, O. K., Goleva, A. A., Andreev, A. A., Cwynar, L. C., Riding, R. T., Forman, S. L., Edwards, T. W. D., Aravena, R., Hammarlund, D., Szeicz, J. M., and Gattaulin, V. N.: Holocene treeline history and climate change across northern Eurasia, Quaternary Research, 53, 302–311, 2000.

Moody, E. G., King, M. D., Schaaf, C. B., Hall, D. K., and Platnick, S.: Northern Hemisphere five-year average (2000-2004) spectral albedos of surfaces in the presence of snow: Statistics computed from Terra MODIS land products, Remote Sensing Of Environment, 111, 337–345, 2007.

Murphy, J. M., Sexton, D. M. H., Barnett, D. N., Jones, G. S., Webb, M. J., and Collins, M.: Quantification of modelling uncertainties in a large ensemble of climate change simulations, Nature, 430, 768–772, 2004.

Notaro, M. and Liu, Z. Y.: Potential impact of the Eurasian boreal forest on North Pacific climate variability, J. Climate, 20, 981–992, 2007.

Notaro, M. and Liu, Z. Y.: Statistical and dynamical assessment of vegetation feedbacks on climate over the boreal forest, Climate Dyn., 31, 691–712, 2008.

O'ishi, R. and Abe-Ouchi, A.: Influence of dynamic vegetation on climate change arising from increasing CO2, Climate Dynamics, 33, 645–663, 2009.

O'ishi, R., Abe-Ouchi, A., Prentice, I. C., and Sitch, S.: Vegetation dynamics and plant CO2 responses as positive feedbacks in a greenhouse world, Geophysical Research Letters, 36, L11 706, 2009.

Otterman, J., Chou, M. D., and Arking, A.: Effects Of Nontropical Forest Cover On Climate, J. Climate Appl. Meteor., 23, 762–767, 1984.

Otto, J., Raddatz, T., and Claussen, M.: Climate variability-induced uncertainty in mid-Holocene atmosphere-ocean-vegetation feedbacks, Geophysical Research Letters, 36, L23 710, 2009a.

Otto, J., Raddatz, T., Claussen, M., Brovkin, V., and Gayler, V.: Separation of atmosphere-ocean-vegetation feedbacks and synergies for mid-Holocene climate, Geophysical Research Letters, 36, L09 701, 2009b.

Petoukhov, V., Ganopolski, A., Brovkin, V., Claussen, M., Eliseev, A., Kubatzki, C., and Rahmstorf, S.: CLIMBER-2: a climate system model of intermediate complexity. Part I: model description and performance for present climate, Climate Dynamics, 16, 1–17, 2000.

Pitman, A. J.: The evolution of, and revolution in, land surface schemes designed for climate models, International Journal Of Climatology, 23, 479–510, 2003.

Pitman, A. J., de Noblet-Ducoudre, N., Cruz, F. T., Davin, E. L., Bonan, G. B., Brovkin, V., Claussen, M., Delire, C., Ganzeveld, L., Gayler, V., van den Hurk, B. J. J. M., Lawrence, P. J., van der Molen, M. K., Muller, C., Reick, C. H., Seneviratne, S. I., Strengers, B. J., and Voldoire, A.: Uncertainties in climate responses to past land cover change: First results from the LUCID intercomparison study, Geophysical Research Letters, 36, L14 814, 2009.

Qu, X. and Hall, A.: What controls the strength of snow-albedo feedback?, Journal Of Climate, 20, 3971–3981, 2007.

Raddatz, T. J., Reick, C. H., Knorr, W., Kattge, J., Roeckner, E., Schnur, R., Schnitzler, K. G., Wetzel, P., and Jungclaus, J.: Will the tropical land biosphere dominate the climate-carbon cycle feedback during the twenty-first century?, Climate Dyn., 29, 565–574, 2007.

Rechid, D., Raddatz, T., and Jacob, D.: Parameterization of snow-free land surface albedo as a function of vegetation phenology based on MODIS data and applied in climate modelling, Theoretical And Applied Climatology, 95, 245–255, 2008.

Renssen, H., Seppa, H., Heiri, O., Roche, D., Goosse, H., and Fichefet, T.: The spatial and temporal complexity of the Holocene thermal maximum, nature geoscience, 2009.

Rimbu, N., Lohmann, G., Lorenz, S. J., Kim, J. H., and Schneider, R. R.: Holocene climate variability as derived from alkenone sea surface temperature and coupled ocean-atmosphere model experiments, Climate Dyn., 23, 215–227, 2004.

Roeckner, E., Bäuml, G., Bonaventura, L., Brokopf, R., Esch, M., M., G., Hagemann, S., Kirchner, I., Kornblueh, L., Manzini, E., Rhodin, A., Schlese, U., Schulzweida, U., and Tompkins, A.: The atmospheric general circulation model ECHAM5. Part I:

Model description., Tech. Rep. Rep. 349, 127 pp., Max Planck Institute for Meteorology, Available from MPI for Meteorology, Bundesstr. 53, 20146 Hamburg, Germany.], 2003.

Roesch, A.: Assessment of the land surface scheme in climate models with focus on surface albedo and snow cover, Ph.D. thesis, Swiss Federal Institute of Technology Zurich, 1999.

Roesch, A. and Roeckner, E.: Assessment of snow cover and surface albedo in the ECHAM5 general circulation model, Journal Of Climate, 19, 3828–3843, 2006.

Rutter, N., Essery, R., Pomeroy, J., Altimir, N., Andreadis, K., Baker, I., Barr, A., Bartlett, P., Boone, A., Deng, H. P., Douville, H., Dutra, E., Elder, K., Ellis, C., Feng, X., Gelfan, A., Goodbody, A., Gusev, Y., Gustafsson, D., Hellstrom, R., Hirabayashi, Y., Hirota, T., Jonas, T., Koren, V., Kuragina, A., Lettenmaier, D., Li, W. P., Luce, C., Martin, E., Nasonova, O., Pumpanen, J., Pyles, R. D., Samuelsson, P., Sandells, M., Schadler, G., Shmakin, A., Smirnova, T. G., Stahli, M., Stockli, R., Strasser, U., Su, H., Suzuki, K., Takata, K., Tanaka, K., Thompson, E., Vesala, T., Viterbo, P., Wiltshire, A., Xia, K., Xue, Y. K., and Yamazaki, T.: Evaluation of forest snow processes models (SnowMIP2), Journal Of Geophysical Research-Atmospheres, 114, D06 111, 2009.

Schaaf, C. B., Gao, F., Strahler, A. H., Lucht, W., Li, X. W., Tsang, T., Strugnell, N. C., Zhang, X. Y., Jin, Y. F., Muller, J. P., Lewis, P., Barnsley, M., Hobson, P., Disney, M., Roberts, G., Dunderdale, M., Doll, C., d'Entremont, R. P., Hu, B. X., Liang, S. L., Privette, J. L., and Roy, D.: First operational BRDF, albedo nadir reflectance products from MODIS, Remote Sensing Of Environment, 83, 135–148, 2002.

Schurgers, G., Mikolajewicz, U., Groger, M., Maier-Reimer, E., Vizcaino, M., and Winguth, A.: Long-term effects of biogeophysical and biogeochemical interactions between terrestrial biosphere and climate under anthropogenic climate change, Global And Planetary Change, 64, 26–37, 2008.

Schwartz, M. D. and Karl, T. R.: Spring Phenology - Natures Experiment To Detect The Effect Of Green-Up On Surface Maximum Temperatures, Monthly Weather Review, 118, 883–890, 1990.

Stein, U. and Alpert, P.: Factor Separation In Numerical Simulations, Journal of the Atmospheric Sciences, 50, 2107–2115, 1993.

Sturm, M., Douglas, T., Racine, C., and Liston, G. E.: Changing snow and shrub conditions affect albedo with global implications, Journal Of Geophysical Research-Biogeosciences, 110, G01 004, 2005.

Texier, D., de Noblet, N., Harrison, S. P., Haxeltine, A., Jolly, D., Joussaume, S., Laarif, F., Prentice, I. C., and Tarasov, P.: Quantifying the role of biosphere-atmosphere feedbacks in climate change: coupled model simulations for 6000 years BP and comparison with palaeodata for northern Eurasia and northern Africa, Climate Dynamics, 13, 865–882, 1997.

Timm, O., Timmermann, A., Abe-Ouchi, A., Saito, F., and Segawa, T.: On the definition of seasons in paleoclimate simulations with orbital forcing, Paleoceanography, doi:10.1029/2007PA001461, 2008.

Wang, S. S.: Dynamics of surface albedo of a boreal forest and its simulation, Ecological Modelling, 183, 477–494, 2005.

Wiscombe, W. J. and Warren, S. G.: A Model For The Spectral Albedo Of Snow .1. Pure Snow, Journal Of The Atmospheric Sciences, 37, 2712–2733, 1980.

Wohlfahrt, J., Harrison, S. P., and Braconnot, P.: Synergistic feedbacks between ocean and vegetation on mid- and high-latitude climates during the mid-Holocene, Climate Dyn., 22, 223–238, 2004.

Wohlfahrt, J., Harrison, S. P., Braconnot, P., Hewitt, C. D., Kitoh, A., Mikolajewicz, U., Otto-Bliesner, B. L., and Weber, S. L.: Evaluation of coupled ocean-atmosphere simulations of the mid-Holocene using palaeovegetation data from the Northern Hemisphere extratropics, Climate Dyn., 31, 871–890, doi:10.1007/s00382-008-0415-5, 2008.

Acknowledgements

First and foremost, I thank Thomas Raddatz for being an excellent supervisor. I am very grateful for his scientific advice and for answering all my questions and encouraging me throughout the last years, particularly when I had my pessimistic moments. I extend sincere thanks to Martin Claussen for the academic supervision of this work, for his time and support, interest, and fruitful discussions. He initiated the project and gave me the opportunity to work on this interesting topic.
Many other people contributed to making my time at the MPI pleasurable and productive: I am very grateful for the technical support I received from Veronika Gayler. Veronika patiently started me out on the modelling framework and helped me with all technical difficulties (and with apples & walnuts). I thank Victor Brovkin for helpful discussions and his scientific advice whenever I needed it. I further thank Jochem Marotzke as my panel chair und the fruitful discussions during the panel meetings.
I very much enjoyed being part of the vegetation/land group ('being a tree' so to speak). At all times, I greatly enjoyed the friendly, cooperative and inspiring atmosphere - thank you to all of you.
My PhD work was funded by the International Max Planck Research School on Earth System Modelling. It has been a pleasure to meet so many fellow students, some of them have become good friends. Many thanks go to Antje Weitz and Cornelia Kampmann for their continuous support, both administratively and morally.
The last three years would not have been that much fun without the help and company of my fellow PhD students, past and present. Thanks especially to Fanny Adloff, Werner Bauer, Jonas Bhend, Anne Dallmeyer, Nils Fischer, Malte Heinemann, Rosina Grimm, Mario Krapp, Julia Pongratz, Florian Rauser, Steffen Tietsche, Freja Vamborg, Aiko Voigt. Thank you for your supporting and/or distracting company, for absorbing frustration, and for making me feel comfortable in Hamburg. And thanks to the WOODSTOCK-team for award-winning climate modelling with hammer and saw. Thanks to Bettina Diallo for transforming my children's drawing into a fancy drawing. I am grateful to Tine Rennert for proofreading this manuscript patiently and studiously. I thank my family for their support in every respect. I thank very warmly Philipp, and Puffi and the gang as well.

Die gesamten Veröffentlichungen in der Publikationsreihe des MPI-M
„Berichte zur Erdsystemforschung“,
„Reports on Earth System Science“,
ISSN 1614-1199

sind über die Internetseiten des Max-Planck-Instituts für Meteorologie erhältlich:

http://www.mpimet.mpg.de/wissenschaft/publikationen.html



ISSN 1614-1199